We are IntechOpen,
the world's leading publisher of
Open Access books
Built by scientists, for scientists

5,000
Open access books available

125,000
International authors and editors

140M
Downloads

Our authors are among the

154
Countries delivered to

TOP 1%
most cited scientists

12.2%
Contributors from top 500 universities

BOOK CITATION INDEX
CLARIVATE ANALYTICS
INDEXED

WEB OF SCIENCE™

Selection of our books indexed in the Book Citation Index
in Web of Science™ Core Collection (BKCI)

Interested in publishing with us?
Contact book.department@intechopen.com

Numbers displayed above are based on latest data collected.
For more information visit www.intechopen.com

Chapter

Beamforming Phased Array Antenna toward Indoor Positioning Applications

Nguyen Thanh Huong

Abstract

Indoor positioning systems based on radio wave have drawn a lot of research interest over the last few decades. One of the positioning methods, Angle of Arrival, locating object based on the relative angle of object to the reference points, requires a directional antenna in order to improve the accuracy of indoor positioning system. From this situation, an eight-port phased array antenna using reflection type phase shifter is designed. The input power is split to each antenna through eight-port Wilkinson power divider with insertion loss of about 11 dB and isolation of about 20 dB. To extract more accurate position, the main beam of phased array antenna can be steered smoothly by a design 18 of a continuous and full 360° reflection type phase shifter with low insertion loss variation. Microstrip patch antennas are used as elements in phased array antenna. The steering of main beam is presented by radiation patterns of phased array antenna, measured in anechoic chamber from −45 to 45° with step 5°. The measurement result shows that the main beam direction is quite close to the desired direction in simulation. In most case, the side lobe level is less than the main lobe about 10 dB.

Keywords: angle of arrival (AoA), antenna array, beamforming, phased array, low loss, phase shifter, steering beam

1. Introduction

Nowadays, positioning has played an important part in daily life and is the foundation for many other applications such as navigation, tracking, location-based services, and games. While outdoor positioning has become widespread and popular with satellite-based navigation systems, that is, GPS, GLONASS, and Galileo, indoor positioning systems have attracted a lot of research interest over the last decade. Indoor localization promises to create a lot of new services such as guiding users in museum, preventing thefts from valuable assets, locating products in supermarkets, navigating in mall, saving power consumption of electronic devices, and so on.

Due to scattering and attenuation of microwave on roofs, walls, and other objects, the systems for outdoor positioning are infeasible solutions when applying to indoor positioning. Instead, indoor positioning systems have been implemented based on several technologies: infrared (IR) [1], bluetooth [2, 3], radio-frequency

identification (RFID) [4], wireless local area networks (WLAN) [5], ultra-wideband [6], ultra-sound [7], magnetic positioning [8], and audible sounds [9]. Among them, WLAN-based approach appears to be among the most suitable solutions owing to its wide range and the popularity of equipment. Nowadays, WLAN devices can be found in almost all civil and commercial properties due to their ease of installation and usage. The number of WLAN devices has reached billions and is continuously increasing day by day, as a result, the study in WLAN-based indoor positioning promise to be applied and spread in the near future. Besides, with the current 5G supports, this indoor positioning technology can even attain to longer reach, greater capacity, high accuracy, and reliability.

For WLAN-based approach, indoor localization techniques are classified into RSS scene analysis, ToA, TDoA, RToF, and AoA [1]. While the highly unstable feature of RSS in indoor environments is the major challenge of RSS scene analysis technique and ToA, TDoA, and RToF are based on a precise clock synchronization of devices, the AoA technique requires a directional antenna design to estimate the relative angle of object to reference points.

There have been several antenna designs for AoA-based indoor localization presented in past few years. Giorgetti and Cidronali [10] introduced a switched-beam directional antenna, including six circular antennas to cover six areas in a room. Rzymowski et al. [11] also introduced an antenna design using 12 passive elements electrically steerable parasitic array radiator antenna with one active monopole in the center of the ground plane. By controlling single-pole, single-throw switches, parasitic elements connect to the ground and act as reflectors, which change the main lobe's directions. With 12 passive elements, this antenna has 12 different directions. Kamarudin et al. [12] proposed reconfigurable antennas using PIN diodes to switch lumped components such as inductors and capacitors in order to change the structure of antennas and switch between four beams. Bui et al. [13] built a switch-beam array antenna based on 4×4 Butler matrix to create four beams toward four angles. It is found that these designs are based on switching between the limited number of predefined beams, which limits the resolution in determining the location of object and leads to significant errors in positioning.

For indoor localization, the system needs to determine the location of object with high accuracy. Therefore, an antenna design with high-resolution steering beam ability is very essential in the AoA technique. As discussed above, the current antenna designs for indoor localization system mainly focus on switched-beam antenna structures. With these structures, the resolution of angle of arrival primarily depends on the number of antenna elements. Therefore, to create a system with high resolution of beam scanning, the number of antennas as well as switching elements such as PIN diode, FET also increases, which makes the system more cumbersome and complex. In order to improve the accuracy for AoA-based indoor localization, the aim of this chapter is to study and develop a phased array antenna at Wi-Fi band (2.4 to 2.484 GHz), capable of finely steering beam without increasing the number of antennas.

This chapter addresses the subject of a beamforming phased array antenna, which plays the vital role for AoA-based indoor positioning system. The array antenna is designed to steer the main beam in high resolution without the increase of antenna elements as well as switching elements. The design of this antenna array has focused on developing the controllable 360° continuous reflection type phase shifter. This chapter is organized as follows. In Section 2, we explain the principles of forming beam and several methods to feed antennas and to control the phase differences for phased array antennas. In Section 3, we discuss the structure of phased array antennas used for practical indoor localization, advancing from

antenna elements, power dividers, feed network, and phase shifters. In Section 4, we verify the performance the printed antenna array by the Vector Network Analyzer and in anechoic chamber.

2. Design factors of beamforming phased array antenna

Phased array antenna is a multiple antenna system in which antenna elements are fed coherently with variable phase or amplitude control to provide for pattern shaping [14]. The concept of phased antenna array was introduced in military applications in the 1940s and first used for military applications for several decades. It improved the reception and transmission patterns of antennas and enabled the antenna system to be electronically steered to receive or transmit information from a particular direction without mechanically moving the structure, which cannot be obtained by any single antenna type. Furthermore, in applications for long distance communication, an antenna design with very high directive characteristics is required. As a single antenna usually provide low directivity and gain with wide radiation pattern [15], an array of antennas with high directivity gain is usually used to meet that demand. Recent growth in civilian radar-based sensors and communication systems has drawn increasing interest in utilizing phased array technology for commercial applications. In most cases, the antenna elements in an array are identical to conveniently adjust the directivity and other parameters of the array. Besides, the antenna elements can be arranged in different geometries to create different beams. The complexity of system increases according to the array geometry. The total beam of the array is a combination of the fields radiated by each antenna elements. The fields of elements will interfere constructively to reinforce in desired directions and interfere destructively to cancel in undesired directions in order to provide directive patterns. The influence of element fields on total beam is considered as array factor and the beam steering principle is based on the change of array factor. In addition, feeding techniques also contribute to the array performance and feed network is the most important component since it supplies the signals to the whole antenna structure and determines the amplitude and phase of electromagnetic waves in order to create the desired beam.

2.1 Array geometry

As mentioned in [15], the geometrical configuration of the overall array may be linear, planar, circular, spherical, etc. For each case, the effective field distribution and mutual coupling will be different from one another. A linear phased array is where the antenna elements are aligned along a straight line, called the array axis. Normally, identical antennas with equal distances are selected in order to simplify calculation as well as beam control. An array of identical elements all of identical magnitude and each with a progressive phased is referred to as a uniform array [15]. The distance between two antenna elements is called element spacing d in **Figure 1a**. For linear phased array, the main beam can only scan along the x-axis, and the angle θ represents the "angle of arrival" of the radio waves. A planar phased array antenna is a set of antennas located in a plane with equal spacing between N elements (d_y) in each column and M elements (d_x) in each row, as shown in **Figure 1b**. By adjusting the magnitude and phase of incoming wave for each antenna, the main beam of this structure can be steered along two x- and y-axis. Therefore, it can provide a 2D angular scan, both horizontal ϕ and vertical θ scans. With this advantage, planar phased array antennas are being used in smart antenna
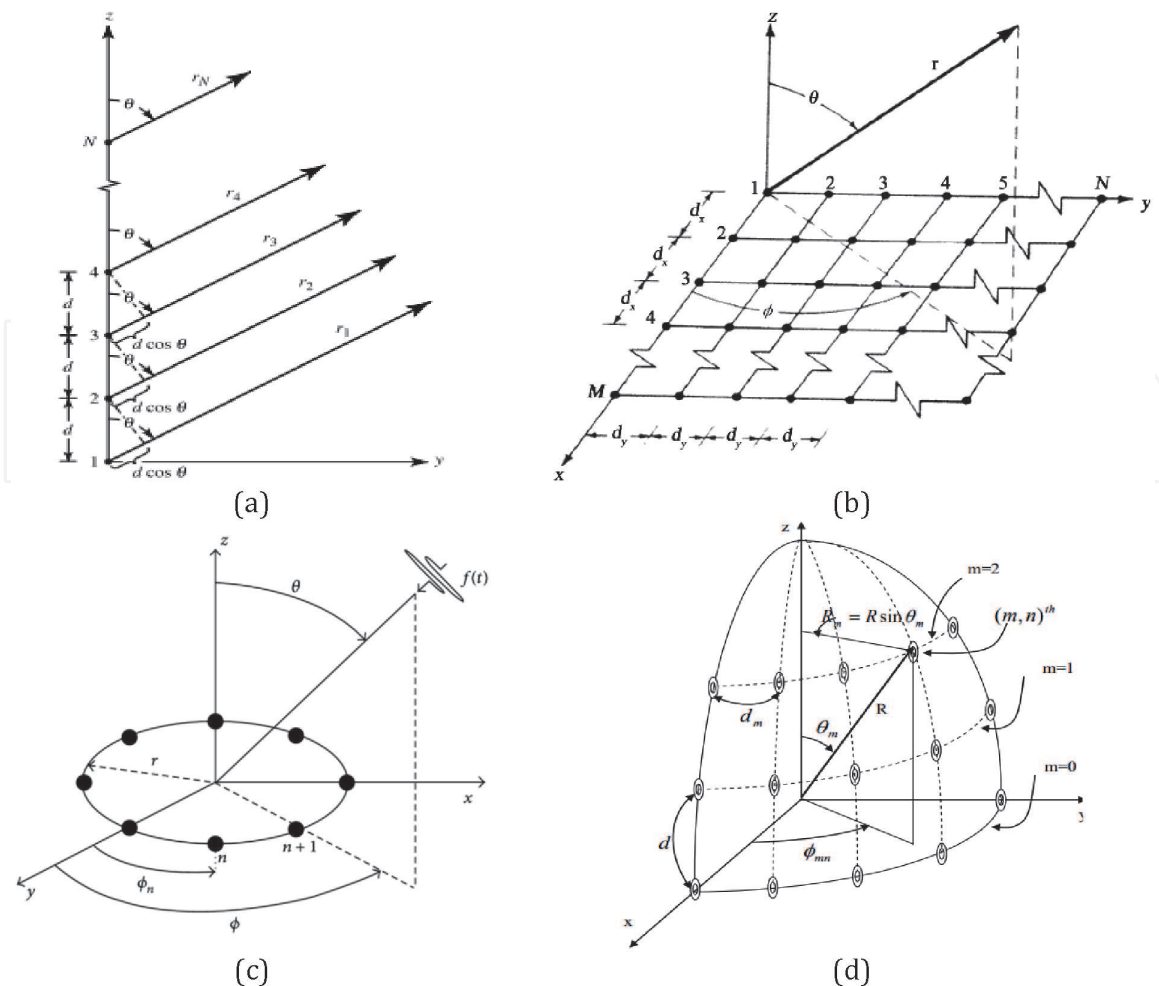
Figure 1.
Phased array geometry: (a) linear, (b) planar, (c) circular, and (d) spherical [15].

and beamforming antenna system. In circular phased array, antennas also lie on the same plane but are arranged on a circular ring of radius r with N equally spaced elements (**Figure 1c**). Circular arrays are basically 1D linear arrays but in circular form and can steer beam in 2D. A spherical phased array consists of antenna elements arranged on the surface of sphere with uniform or non-uniformly spacing (**Figure 1d**). The element spacing is defined as the distance between two adjacent elements along the curved surface. With such geometry, spherical phased array may radiate in any direction and achieve omnidirectional or isotropic coverage. However, due to difficulties in model, design as well as fabrication, this geometry seems to not receive much less attention than above geometries.

2.2 Array factor

Another important factor – Array Factor (*AF*) depends on some parameters such as the number of antennas in array, geometrical arrangements, relative magnitude, phase difference, and element spacing. It is a mathematical factor representing the relationship between total field of array and the field of single element. If E_s is the field of a single antenna and *AF* is the array factor, the total field E_{total} at the far-field of the array can be calculated as [15]:

$$E_{total} = E_s \times AF \tag{1}$$

In case the array of two dipole antennas with element spacing $d = \frac{\lambda}{4}$, the total fields are different corresponding to different phase excitation β shown in **Figure 2**.
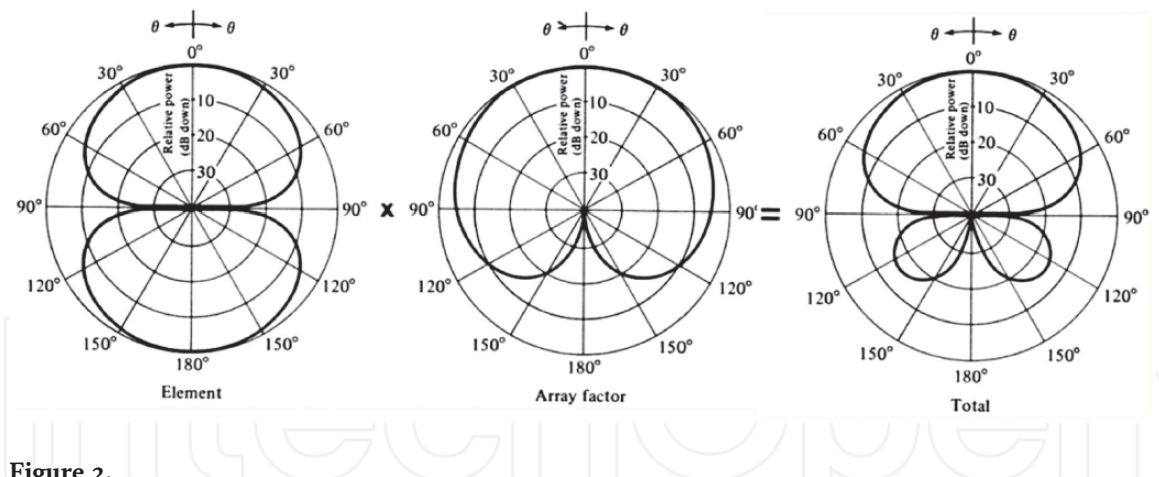
Figure 2.
Total field patterns of two dipole antenna array with λ/4 element spacing and different phase excitation β = −90° [15].

If a linear array has uniform amplitude, distances between two adjacent elements are identical with identical powers traveling to antennas. The *AF* is given as

$$AF = \sum_{n=1}^{N} e^{j(n-1)(kd\ cos\theta + \beta)} \tag{2}$$

where N is the number of antenna elements, d is the element spacing, β is the phase difference of incident waves to antennas, and θ changes from 0 to 2π. The maximum value of array factor is at an angle of $\theta_m = cos^{-1}\left(\frac{\lambda\beta}{2\pi d}\right)$, which enables to control the maximum value of *AF* through controlling the phase difference β. That is the method to steer the main beam in the phased array antenna system. For AoA-based indoor localization, the use of uniform amplitude and spacing linear array is enough. For non-uniform amplitude linear array, planar array, circular array, and spherical array, *AF* is quite complicated and not really necessary but already introduced in [10, 11].

2.3 Grating lobe

When steering main beam toward the desired direction, some side lobes happen to be substantially larger in amplitude and reach the level of the main lobe. The lobe of maximum radiation toward unintended direction is known as a grating lobe which is undesirable in phased array antenna applications. During the transmission, if the energy does not focus in the desired direction, that means it is allocated in the direction of the grating lobes, the transmission distance is significantly reduced. In smart antenna systems where the user's direction is determined, the presence of grating lobes can cause the system to misidentify the user that means while transmitting, unwanted users are also treated as expected user, thus it affects information security or interferes other users. In a whole, to avoid the grating lobes, element spacing d is required to meet the following condition:

$$\frac{d}{\lambda} \leq \frac{1}{1 + |cos\theta|} \tag{3}$$

where λ is the wavelength of operating frequency and θ is the angle between main beam direction and z-axis **Figure 1a**. However, in this chapter, the angle θ = 90° is used as original angel of main beam direction, so angle of main beam will be $(\theta - 90°)$. The scanning main beam angle range is designed from −60 to 60°.

Expression (3) indicates that element spacing *d* in this case is smaller than 0.53λ. Therefore, to avoid grating lobes in scanning angle sector from −60 to 60°, an element spacing not more than 0.53λ is chosen.

2.4 Mutual coupling

When signals are transmitted to antenna arrays, the antenna elements will interfere each other, which is the so-called mutual coupling effect. The amount of coupling depends on the radiation characteristic, relative orientation of each antenna and spacing between elements. As discussed in [15], even if both antennas are transmitting, partial energy radiated will be received by other antennas because of the directional characteristics of practical antennas. Part of the incident energy on antenna elements may be backscattered in different directions, thereby allowing them to behave as secondary transmitters. In many cases, it is very complex to analyze and difficult to predict this effect but the coupling must be taken into account because of its significant contribution.

When two radiating elements are positioned along the E-plane, very small spacing exhibits the smallest coupling isolation, while the H-plane exhibits the small coupling for large spacing [15]. By selecting the correct distance, these fields can be decomposed to surface waves, and the spacing at which on plane coupling overtakes the other one also depends on the electrical properties and the geometrical dimensions of the microstrip antenna. In general, the element spacing should be designed to reduce the adverse effects of mutual coupling. According to [16], the spacing is recommended to be between 0.33λ and 0.5λ.

2.5 Feed network

The angle of radiation beams mainly depends on the range of phase difference at the feed lines to the antenna array. Meanwhile, the phase difference is directly generated from the feed network. In electronically scanned arrays or phased arrays, the feed networks for phase difference generation are typically realized using microwave circuit types such as Hybrid Coupler, Delay Line, Crossover, Power Divider, Phase Shifter, ... Generally, all types of feed networks can be classified into the categories: constrained feeds, space feeds, and hybrid feeds. In an example for the space feed network, a lens array is fed by a single horn antenna located at an expected distance from the array [14] with the phase control at every element in the lens. The main advantage of this configuration is to reduce the cost and weight of the system compared with using hybrid feed, therefore it is applicable to lower cost ground-based arrays as well as very large space-based radar and communication system. However, this configuration is quite complex and requires the precision mechanical system to use the phase control at the objective aperture. Therefore, we select constrained feed which is commonly used for antenna array. The constrained feed can then be categorized into two basic types: series feed and parallel feed.

In series feed, antenna elements are placed in series along the feed line, and phase shifters can be inserted series either antennas or feed line, as shown in **Figure 3a**. The input signal is fed from one end of the feed network and then coupled serially to each antenna element. The compactness and low loss are two main advantages that make series feed more attractive than parallel feed. Additionally, the number of required phase shifters is also less than ones in parallel feed. However, bandwidth limitation is the main disadvantage of series feed. As the feed line is also treated as a delay line, the phase shifts on feed line are different at different frequencies. Therefore, the series feed only operates at designed frequency. Moreover, when phase shifter is placed on the feed line, the loss through
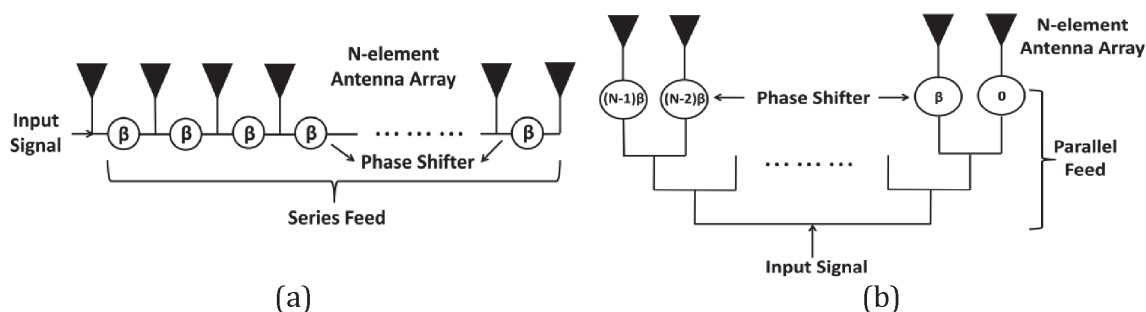
Figure 3.
(a) Series feed network for phased array antenna; (b) parallel feed network for phased array antenna [14].

phase shifters is also cumulative, which can be an issue in the design of array with a large number of elements. Calculating and controlling the phase shift value of the phase shifters become elaborate as they depend on the length of the feed lines.

In parallel feed, which are often called corporate feeds, the input signal is divided in a parallel tree network to all the antenna elements as shown in **Figure 3b**. The parallel feed is composed of power dividers and phase shifters followed by antenna elements. Power dividers split input signal to N signals with same amplitudes and same phases at output ports, then phase shifters control phase shift to each antenna. Thanks to the parallel structure, lengths of transmission lines do not affect phase shift. Therefore, it eliminates the major disadvantage of series feed, operating at only one frequency. Furthermore, because of parallel structure, the phase shifts and losses of phase shifters do not affect each other, which lead to simpler control circuit. However, the disadvantage of parallel feed is cumbersome as discussed above. Moreover, in applications requiring long transmission, transceiver modules including power amplifier, low noise power amplifier, and switch, are used. Sometimes, in array antenna system forming the beam based on amplitude control, power amplifiers with variable gain ability are needed. In practice, variable
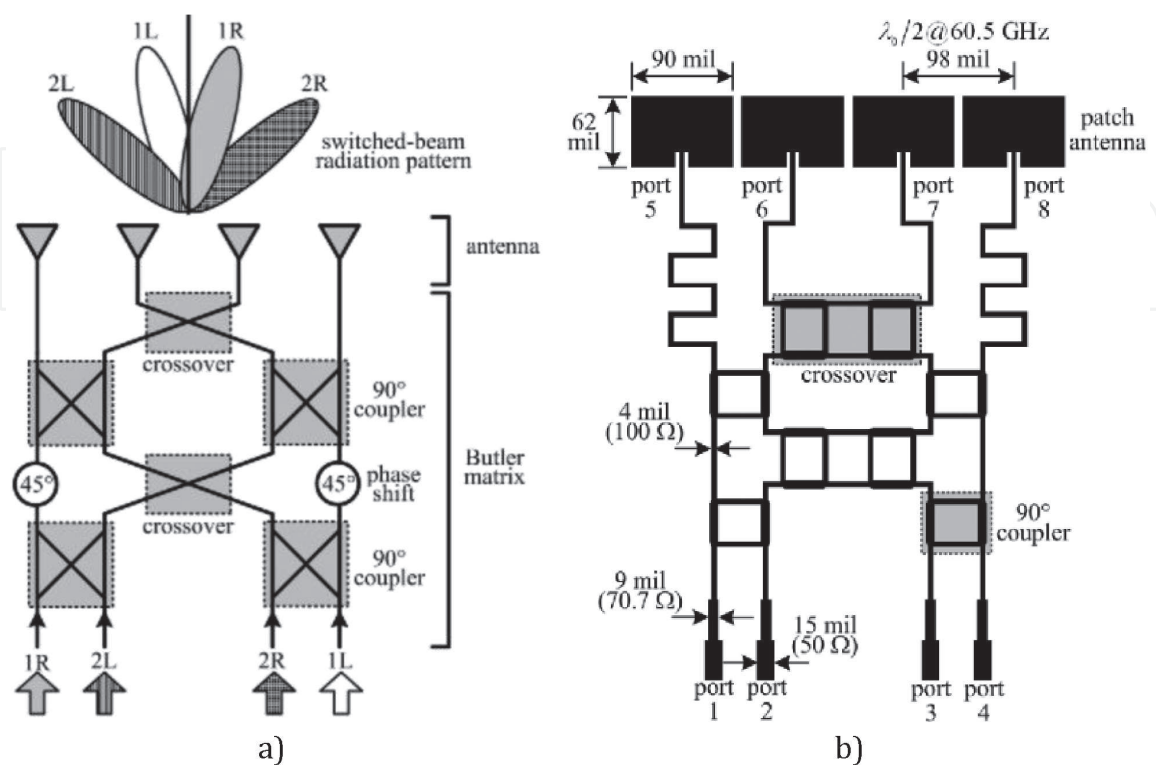
Figure 4.
4 × 4 Butler matrix network [20].

gain also enables to compensate the loss on phase shifter, of which loss value is not small.

Butler matrix is also an approach usually studied in phased array antennas [17–19]. The Butler matrix is a type of beamforming network and first described by Jesse Butler and Ralph Lowe in [20]. It has N inputs and N outputs; with N is usually 4, 8, and 16. One input signal fed from one of input ports goes through components of Butler matrix like couplers, phase shifters, crossovers in order to create phase difference of wave at N output ports, which combines with antenna elements to create beams with different predefined directions, as shown in **Figure 4**. Because beam direction is predefined, this system is also considered as a switched beam system. Nevertheless, there are two main drawbacks when using Butler matrix. First of all, the complexity and dimension significantly increase when N increases. That is why Butler matrix network is hardly designed with the number of input ports of 16 or more. Secondly, the number of beams is limited. With N inputs, this system can only create N beams with different directions, hence it is not suitable to provide beams with high resolution scan angle.

3. Practical phased array antenna design for indoor positioning

The indoor localization and positioning system depend considerably on the phased array antenna structure. The structure as well as parameters of phased array antenna such as array geometry, element spacing, and feed network needs to be carefully defined. For indoor positioning, we only care about the location of users and ignore altitude information, hence a linear array structure with 2D scanning can fully meet this requirement. Other architectures such as planar array, circular array, and spherical array are also options, but they make the system much more complex and cumbersome. With a straightforward beam steering principle, the uniform amplitude and spacing linear array is chosen.

Regarding the element spacing of linear array antenna system, it should be a suitable value in order to limit the mutual coupling, avoid grating lobes, and increase the directivity. As mentioned in Section 2, to reduce the adverse effects of mutual coupling, element spacing should be from 0.33λ to 0.5λ. With respect to the usage, the antenna system is aimed to be located at the corner of the room and the user will move inside the room, yielding the main beam angle from -45 to $45°$. Thus, from Eq. (3), the element spacing is chosen to be less than 0.58λ to prevent the appearance of grating lobes when scanning main beam angle from -45 to $45°$. In [21], Rabinovich and Alexandrov show the relationship between directivity and element spacing of array antenna (**Figure 5**). When element spacing d is less than wavelength λ, the directivity is proportional to d/λ. To sum up, the element spacing equals to half wavelength in my antenna system. Finally, with advantages compared to serial feed and butler matrix, the parallel feed network is selected for this beamforming phased array.

3.1 Power divider

A parallel feed network is composed of power dividers and phase shifters. The incident wave is split to multiple ports through power dividers. With design of uniform amplitude and spacing linear array, the power should be equally split to each output port. If the phases of outgoing waves are identical, the compensation of phase will not be required. In microwave, reducing the loss enables more power to feed into antennas, which increases the transmission range. Finally, the mismatch in microwave circuits causes the reflection waves, which can play another role as
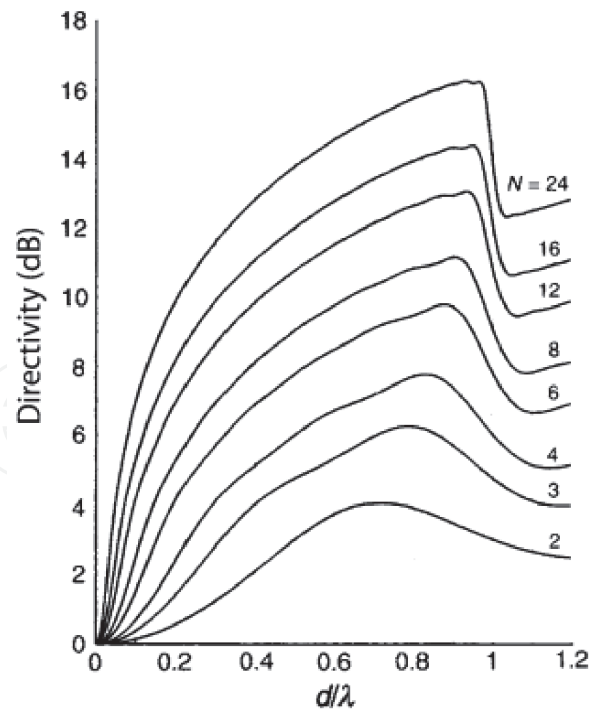
Figure 5.
Directivity as a function of the element spacing of linear array antenna [21].

incoming waves at output ports. Therefore, if output ports of power divider are highly isolated to each other, the reflected waves will not affect other ports.

Power divider is a passive component to split the input signal into two or more lower power output signals. Power dividers usually provide in-phase output signals with both equal power division ratio (3 dB) and unequal power division ratios. As described in [22], T-junction and Wilkinson are two kinds of most popular power dividers. While the T-junction dividers have some disadvantages related to impedance matching, power loss or isolation, the Wilkinson Power Divider (WPD) can simultaneously solve these problems. The WPD appears lossless when the output ports are matched. The structure of WPD, shown in **Figure 6**, comprises two quarter-wave transmission lines with impedance of $\sqrt{2}Z_0$ and a $2Z_0$ lumped-element resistor at the end. To analyze this circuit, the "even-odd" mode analysis
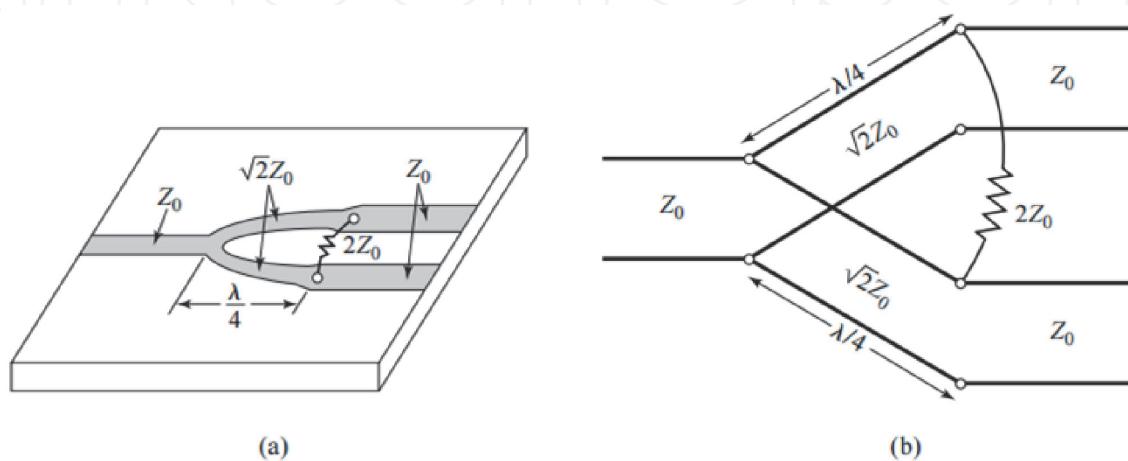
Figure 6.
The Wilkinson power divider: (a) microstrip line configuration, (b) equivalent transmission line circuit [22].

technique is often used, and the scattering matrix calculation is represented in [22]. Finally, the scattering matrix of WPD is:

$$S = \frac{-1}{\sqrt{2}} \begin{bmatrix} 0 & j & j \\ j & 0 & 0 \\ j & 0 & 0 \end{bmatrix} \tag{4}$$

We can see that the power from input port is split into two output ports without power loss on transmission line, there is no reflection wave from output ports and output ports are completely isolated. With advantages of WPD over T-junction dividers, the WPD is utilized as the power divider for feed network of antenna array. In [22], professor Pozar introduced the N-way WPD (**Figure 7**) in which the transmission line has impedance depending on the number of output ports. This circuit can be matched at all ports, with isolation between all ports. The drawback of this structure is to use crossovers for the resistors for $N \geq 3$, which makes fabrication difficult in planar form. The WPD is arranged in cascade structure for low loss and better isolation, shown in **Figure 8**. Two-way WPD is connected together by 50 Ω transmission
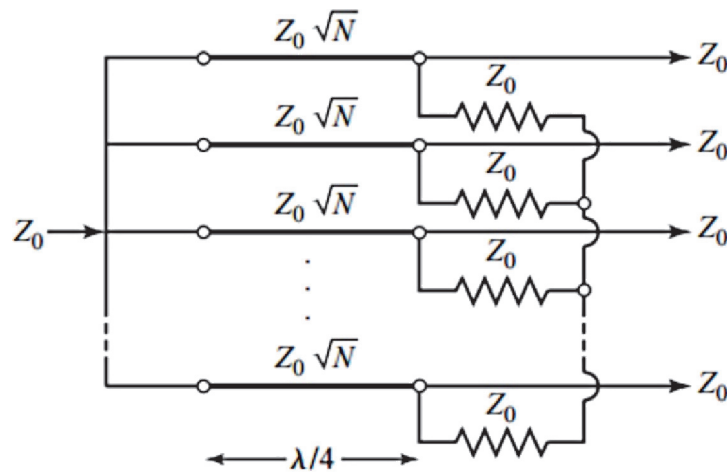
Figure 7.
An N-way, equal-split Wilkinson power divider [22].
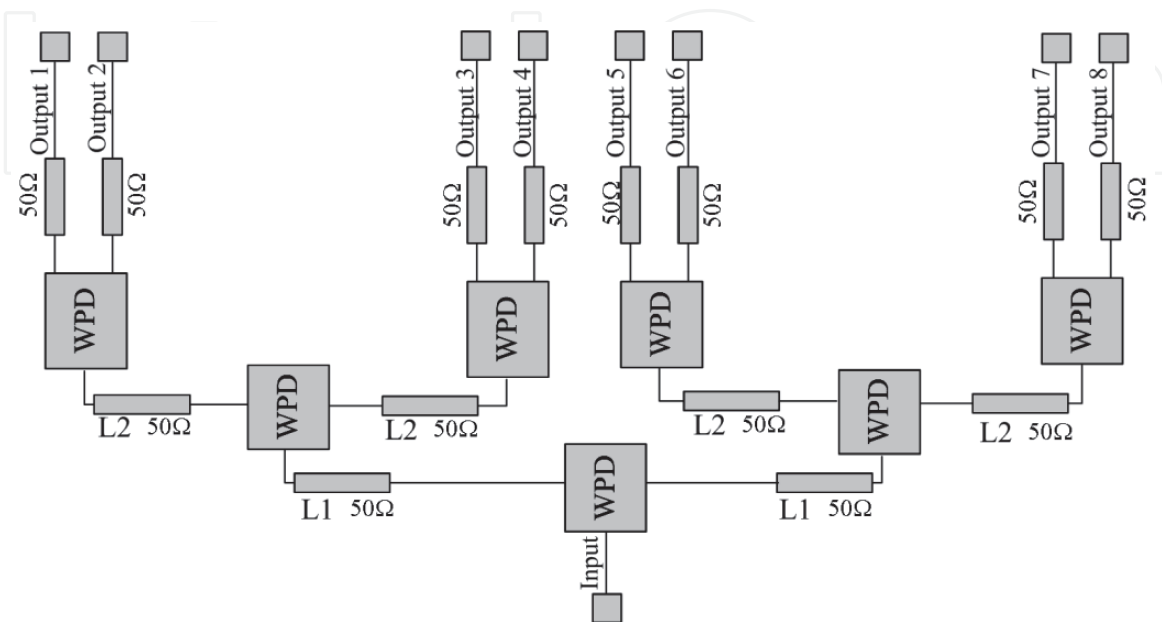
Figure 8.
The eight-way equal-split Wilkinson power divider [23].

lines in a three-stage structure. The 50 Ω transmission lines allow to arbitrarily adjust distances between output ports in order to satisfy the dimension of phase shifters and element spacing between antennas in phased array antenna system.

3.2 Phase shifter

3.2.1 Phase shifter theoretical calculation

In parallel feed network, the main role of phase shifter is to create the phase difference of waves coming to the antennas in order to scan a beam or to reconfigure a beam shape. Three characteristics are required for this phase shifter. Firstly, it must be capable of shifting phase of waves in full 360° range in order to meet all of the demands of the phase difference in phased array antenna system. Secondly, continuously shifting makes it possible to create any phase, which enables steering main beam with high resolution. Finally, with a uniform amplitude and spacing linear array, when power divider equally splits power to output ports, a phase shifter with low insertion loss variation is very important. Without this property, our linear array should be treated as a non-uniform amplitude linear array, which is more complex in beam steering principle.

Depending on the required output, phase shifters are classified into analog phase shifter and digital phase shifter. Digital phase shifters with semiconductor components such as PIN diode and FET switch predefined states to provide predetermined phase shift. The phase shift, generated by this type, has high accuracy. However, structure of this type will become cumbersome to meet high-resolution demands. With high resolution, the number of predefined states increases, resulting in the expansion of the number of switching elements as well as size of controller for them. Meanwhile, analog phase shifter with the use of varactors or Schottky diodes can continuously change the phase shift. These diodes have capacitance depending on the bias voltage, for this reason, they can be used as electrically variable capacitor in tuned circuit accordingly. By shifting the phase continuously, this type can provide high-resolution phase shift without changing its hardware structure. However, less accuracy and relatively narrow bandwidth are drawbacks of this type. On implementing a microwave phase shifter, these disadvantages must be enhanced for better performance.

There exist four types of phase shifters, as shown in **Figure 9**. One of the digital phase shifter, the switched-line one, adopts delay lines and switching elements to generate time delay differences.

The phase shift depends only on transmission line length; therefore, it is very stable over time and temperature. A basic schematic of switched line phase shifter is shown in **Figure 9a**. The second type, switched network phase shifter (**Figure 9b**), is similar to switched line phase shifter but delay lines are replaced by networks composed of inductors and capacitors. The dimension of this type does not change as much as switched line phase shifter, besides this type is suitable for low frequency design. Loaded line phase shifters (**Figure 9c**) are loaded with a shunt reactance that is electrically shortened or lengthen by PIN diode or FET in order to get the desired phase shift. This type has advantages of simplicity and low insertion loss for phase shift less than 45°. However, for larger values of phase shift, high sensitivity is required in order to increase insertion loss. Therefore, this type is only suitable for phase shift less than 45°. Reflection type phase shifter comprises a 3-dB hybrid couple and two tunable loads, as shown in **Figure 9d**. By selecting the appropriate load, this type can shift more than 360° continuously and has low insertion loss, like in [24–26]. From requirement of phase shifter, it is obvious that reflection type phase shifter with full 360° and continuous phase shift is the most appropriate choice for this phased array antenna system.
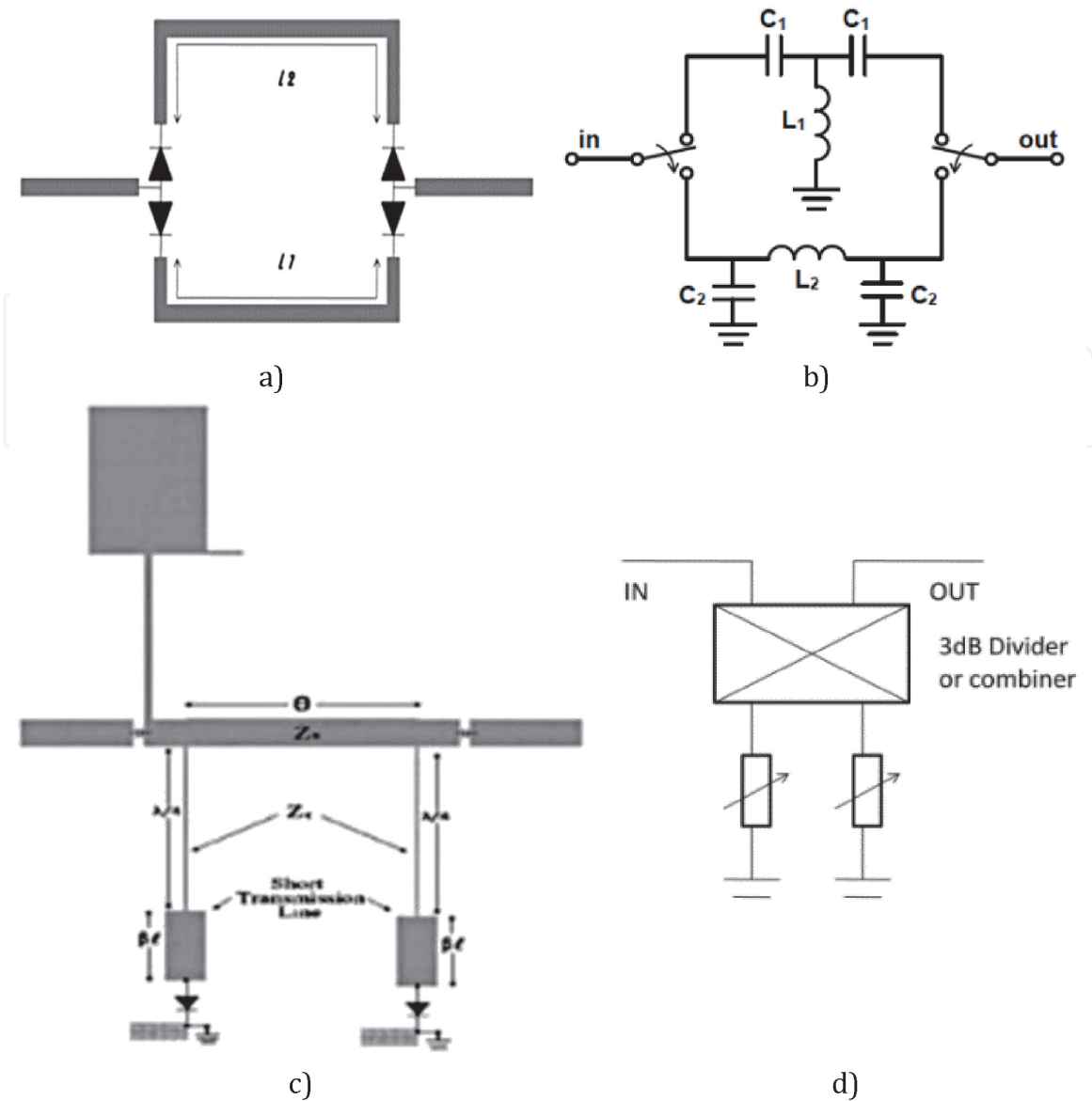
Figure 9.
Types of phase shifter: (a) switched line; (b) switched network; (c) loaded line; (d) reflection type [24–26].

The Reflection Type Phase Shifter (RTPS), an electrically adjustable phase shift, is made up of a 3-dB hybrid coupler combined with some components such as capacitors, resistors, transmission line, and varactors to eliminate the reflected wave at input port and shift phase of wave at output port. The 3-dB hybrid coupler is a 4-port network with all ports matched to the reference impedance of 50 Ω. When stimulating at port 1, incoming wave transmits to port 3, port 4, and is
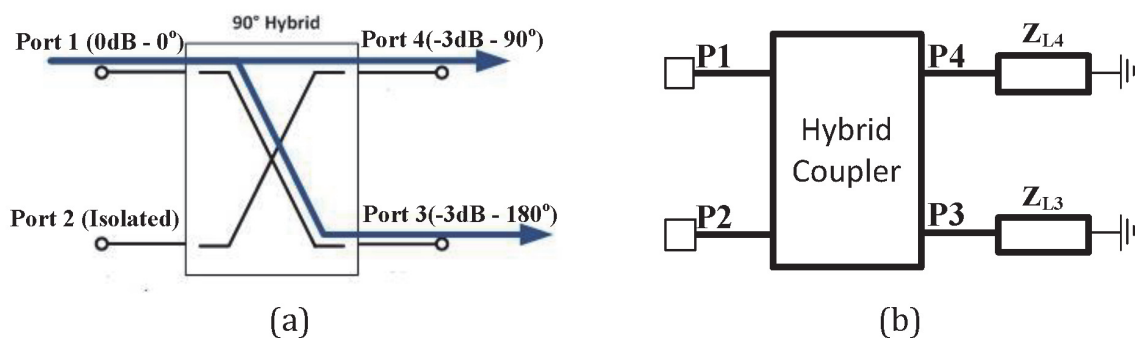
Figure 10.
(a) 3-dB hybrid coupler; (b) structure of RTPS.

suppressed at port 2. The amplitude of waves at ports 3 and 4 equal to $\frac{1}{\sqrt{2}}$ one of incoming wave at port 1 and phase of waves at port 3 and 4 shift 90° and 180° compared with one at port 1, respectively (**Figure 10a**).

In mathematical model, 3-dB hybrid coupler is characterized by a scattering matrix that represents voltage relationship between incoming (V+) and reflected (V) waves at different ports.

$$[V^-] = [S][V^+] \tag{5}$$

$$[S] = \frac{1}{\sqrt{2}} \begin{bmatrix} 0 & 0 & -j & -1 \\ 0 & 0 & -1 & -j \\ -j & -1 & 0 & 0 \\ -1 & -j & 0 & 0 \end{bmatrix} \tag{6}$$

Here, S_{ij} is ratio of the reflected wave at port i to the incoming wave at port j when there is only input wave from port j.

$$[S_{ij}] = \left.\frac{V_i^-}{V_j^+}\right|_{V_k^+=0,k\neq j} \tag{7}$$

To be more specific, we have:

$$\begin{bmatrix} V_1^- \\ V_2^- \\ V_3^- \\ V_4^- \end{bmatrix} = \begin{bmatrix} \left(\frac{-j}{\sqrt{2}}V_3^+\right) + \left(\frac{-1}{\sqrt{2}}V_4^+\right) \\ \left(\frac{-j}{\sqrt{2}}V_3^+\right) + \left(\frac{-1}{\sqrt{2}}V_4^+\right) \\ \left(\frac{-j}{\sqrt{2}}V_1^+\right) + \left(\frac{-1}{\sqrt{2}}V_3^+\right) \\ \left(\frac{-1}{\sqrt{2}}V_1^+\right) + \left(\frac{-j}{\sqrt{2}}V_2^+\right) \end{bmatrix} \tag{8}$$

Considering the reflection coefficient (Γ) generated by the load, the reflection coefficient is determined from the load impedance and the source impedance.

$$\Gamma = \frac{V^-}{V^+} = |\Gamma|e^{j\phi} \tag{9}$$

From the two components constituting the RTPS, the 3-dB hybrid coupler and the reflective load mentioned above, the model of RTPS is shown as in **Figure 10b**, with port 1 as incoming port, port 2 as outgoing port, and two loads Z_{L3} and Z_{L4} at port 3 and 4, respectively. The phase shift of RTPS is the phase difference between outgoing wave at port 2 compared with incoming wave at port 1. Suppose there is only an incoming wave at port 1. When passing through the 3-dB hybrid coupler, from (8), waves at ports 3 and 4 are:

$$V_3^+ = -\frac{j}{\sqrt{2}}V_1^+; V_4^+ = -\frac{1}{\sqrt{2}}V_1^+ \tag{10}$$

Because of appearance of ZL3 load at port 3, there is wave reflection with reflection coefficient Γ3. Therefore, from (9) and (10), the reflection wave at port 3 is:

$$V_3^- = \Gamma_3 V_3^+ = -\frac{j}{\sqrt{2}} \Gamma_3 V_1^{+\cdot} \tag{11}$$

Similarly, we have the reflected wave at port 4:

$$V_4^- = \Gamma_4 V_4^+ = -\frac{j}{\sqrt{2}} \Gamma_4 V_1^+ \tag{12}$$

The reflected waves at ports 3 and 4 can be also regarded as incoming waves from ports 3, 4 transmitting to ports 1 and 2. We set $V_3'^+$ and $V_4'^+$ as incoming wave at ports 3 and 4, respectively. We have:

$$V_3'^+ = V_3^- = -\frac{j}{\sqrt{2}} \Gamma_3 V_1^+ \tag{13}$$

$$V_4'^+ = V_4^- = -\frac{j}{\sqrt{2}} \Gamma_4 V_1^+ \tag{14}$$

These two waves transmit to ports 1 and 2 through 3 dB hybrid coupler, and outgoing waves from ports 1 and 2 are calculated from (6), (11), and (12) as follows:

$$V_1^- = -\frac{j}{\sqrt{2}} V_3'^+ - \frac{1}{\sqrt{2}} V_4'^+ = -\frac{1}{2}\left(\Gamma_3 V_1^+ - \Gamma_4 V_1^+\right)$$

$$V_2^- = -\frac{1}{\sqrt{2}} V_3'^+ - \frac{j}{\sqrt{2}} V_4'^+ = \frac{j}{2}\left(\Gamma_3 V_1^+ + \Gamma_4 V_1^+\right) \tag{15}$$

For the phase shifter, we wish that there is no reflected wave at port 1. Therefore, $\Gamma_3 = \Gamma_4$ enables us to eliminate the reflected wave at port 1. From (9) and (13), choosing $Z_{L3} = Z_{L4}$ makes $\Gamma_3 = \Gamma_4 = \Gamma$ and outgoing wave at port 2 as $V_2^- = j\Gamma V_1^+$. Finally, the forward voltage gain S_{21} of RTPS will be as follow:

$$S_{21} = \frac{V_2^-}{V_1^+} = j\Gamma = j|\Gamma|e^{j\phi} = |\Gamma|e^{j\left(\frac{\pi}{2}+\phi\right)}$$

$$\angle S_{21} = \frac{\pi}{2} + \phi \tag{16}$$

3.2.2 Design of reflection type phase shifter

The reflection type phase shifter (RTPS) is a phase shifter, empowering continuous change of the phase of wave without the need to change hardware structure, based on the change in capacitance of varactors. **Figure 11** shows the principle diagram of the RTPS, which consists of a 3-dB hybrid coupled and reflection loads X_L putting at ports 3 and 4. Waves enter port 1 and go out port 2.
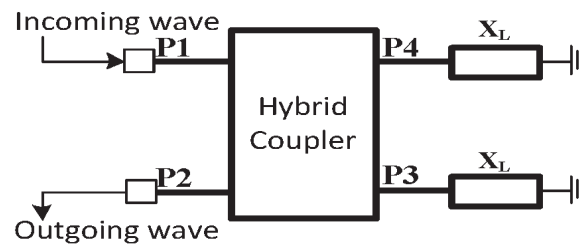
Figure 11.
Schematic diagram of RTPS.

When putting reactive loads to ports 3 and 4, the reflection coefficient is:

$$\Gamma = \frac{jX_L - Z_0}{jX_L + Z_0} = \frac{(jX_L - Z_0)^2}{(jX_L + Z_0)(jX_L - Z_0)} = \frac{1}{Z_0^2 + X_L^2}(jX_L - Z_0)^2$$

$$= \frac{1}{Z_0^2 + X_L^2}\left(\sqrt{Z_0^2 + X_L^2}e^{jarctan\left(-\frac{X}{Z_0}\right)}\right)^2 = e^{j2arctan\left(-\frac{X}{Z_0}\right)} \tag{17}$$

From (14) and (15), the phase shift of RTPS with reactive loads is:

$$\angle S_{21} = \frac{\pi}{2} - 2\,arctan\left(\frac{X_L}{Z_0}\right) \tag{18}$$

From (16), we found that the range of phase shift values $\angle S_{21}$ entirely depends on the capacitance range of varactors, which limits the phase shift range. To be more specific, in order to achieve the 360° phase shift, theoretically, the capacitance of varactors must reach infinity, which is impossible. Therefore, RTPS cannot get the full 360° with only one varactor on reflection loads. To overcome the above problem, the reflection load structure shown in **Figure 12** is employed. This endows us to choose the appropriate capacitance range, thus selecting the suitable varactors and its voltage as follows:

Based on the transmission line impedance theory [27], because Z_{T2} is a quarter-wavelength transmission line, the equivalent impedance of Z_{T2} and D_2 is:

$$Z_2 = \frac{Z_{T2}^2}{Z_d} \tag{19}$$

The equivalent circuit becomes (**Figure 13**):

Similarly, Z_{T1} is also a quarter-wavelength, so the equivalent impedance is:

$$Z_L = Z_{T1}^2\left(\frac{1}{Z_d} + \frac{1}{Z_2}\right) \tag{20}$$
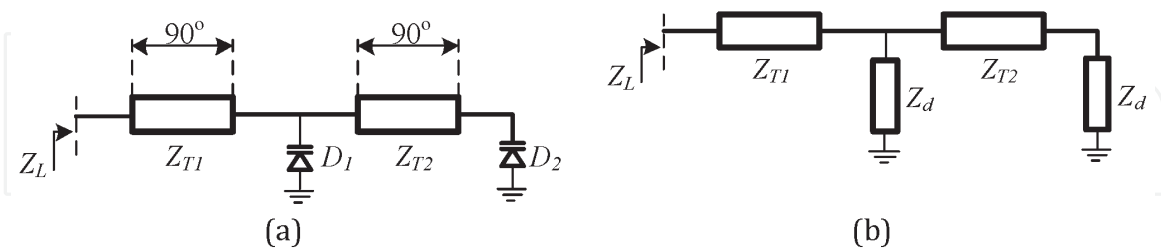
Figure 12.
(a) Reflection load of RTPS; (b) the equivalent circuit of reflection load.
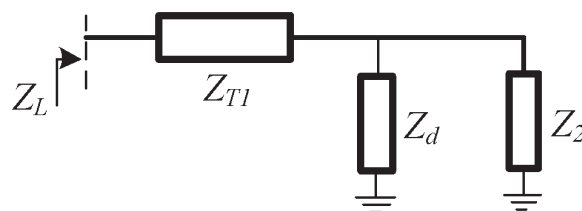
Figure 13.
The equivalent circuit of final RTPS.

Substitute (17) to (18):

$$Z_L = Z_{T1}^2 \left(\frac{1}{Z_d} + \frac{1}{Z_2} \right) = Z_{T1}^2 \left(\frac{1}{Z_d} + \frac{Z_d}{Z_{T2}^2} \right) = \frac{Z_{T1}^2}{Z_{T2}^2} \frac{Z_{T2}^2 + Z_d^2}{Z_d} \tag{21}$$

On the other hand, the impedance of the capacitance diodes is:

$$Z_d = j\omega L_s + \frac{1}{j\omega C_d} = j \left(\omega L_s - \frac{1}{\omega C_d} \right) = jX_d \tag{22}$$

Substitute (20) to (19):

$$Z_L = jX_L = \frac{Z_{T1}^2 (Z_{T2}^2 - X_d^2)}{Z_{T2}^2 jX_d} = j \frac{Z_{T1}^2 (X_d^2 - Z_{T2}^2)}{Z_{T2}^2 X_d} \tag{23}$$

Substitute (21) to (16):

$$\angle S_{21} = \frac{\pi}{2} - 2\arctan\left(\frac{X_L}{Z_0} \right) = \frac{\pi}{2} - 2\arctan\left(\frac{Z_{T1}^2 (X_d^2 - Z_{T2}^2)}{Z_{T2}^2 X_d Z_0} \right) \tag{24}$$

In order to get 360° phase shift, we have:

$$\angle S_{21}\big|_{X_{dmin}} = \angle S_{21}\big|_{X_{dmax}}$$

$$\Leftrightarrow \frac{\pi}{2} - 2\arctan\left(\frac{Z_{T1}^2 (X_{dmin}^2 - Z_{T2}^2)}{Z_{T2}^2 X_{dmin} Z_0} \right) = \frac{\pi}{2} - 2\arctan\left(\frac{Z_{T1}^2 (X_{dmax}^2 - Z_{T2}^2)}{Z_{T2}^2 X_{dmax} Z_0} \right)$$

$$\Leftrightarrow \frac{Z_{T1}^2 (X_{dmin}^2 - Z_{T2}^2)}{Z_{T2}^2 X_{dmin} Z_0} = \frac{Z_{T1}^2 (X_{dmax}^2 - Z_{T2}^2)}{Z_{T2}^2 X_{dmax} Z_0}$$

$$\Leftrightarrow X_{dmin} - \frac{Z_{T2}^2}{X_{dmin}} = X_{dmax} - \frac{Z_{T2}^2}{X_{dmax}}$$

$$\Leftrightarrow (X_{dmin} - X_{dmax}) \left(1 + \frac{Z_{T2}^2}{X_{dmin} X_{dmax}} \right) = 0$$

Since $X_{dmin} \neq X_{dmax}$, we have:

$$Z_{T2}^2 = -X_{dmin} X_{dmax} \tag{25}$$

Thus, by calculation of Z_{T2} satisfying (23), we will have 360° phase shift. From (23), we have: $X_{dmin} X_{dmax} < 0$

$$\Leftrightarrow \left(\omega L_s - \frac{1}{\omega C_{dmin}} \right) \left(\omega L_s - \frac{1}{\omega C_{dmax}} \right) < 0$$

$$\Leftrightarrow \begin{cases} C_{dmin} < \dfrac{1}{\omega^2 L_s} \\[2mm] C_{dmax} > \dfrac{1}{\omega^2 L_s} \end{cases}$$

$$\Rightarrow \frac{1}{\omega^2 L_s} \in [C_{dmin}; C_{dmax}] \tag{26}$$

At 2.45 GHz, for impedance matching, the varactor diode SMV1247, package type SC-79 of Skyworks is chosen with L_s = 0.7nH. To simplify the voltage controller of the varactors, the model capacitance range of SMV1247 from 8.5 pF to 0.7 pF is selected corresponding to the voltage range from 0 V to 5 V. From (23), Z_{T2} = 15 Ω.

For the impedance of Z_{T1}, besides calculating the entire phase shift, the change of phase shift needs to be taken into account. It is desired that the relationship between the control voltage and the phase shift becomes as close to linear as possible, so that controlling phase shift with small resolution is easier. Thus, it is important to examine the expression $\frac{d\angle S_{21}}{dV_R}$ where V_R is the bias voltage of varactors and $\angle S_{21}$ is the phase shift. As for SMV1247, the relationship between bias voltage and capacitive value as follows:

$$C_d = \frac{C_{J0}}{\left(1 + \frac{V_R}{V_J}\right)^M} + C_P \qquad (27)$$

where C_{J0} = 8.47 pF, V_J = 80 V, M = 70, C_P = 0.54 pF are package parameters from varactor SMV1247's datasheet.

Substitute (25) to (22), the relational expression between $\angle S_{21}$ and V_R is:

$$\begin{cases} \angle S_{21} = \frac{\pi}{2} - 2\,arctan\left(\frac{Z_{T1}^2\left(X_d^2 - Z_{T2}^2\right)}{Z_{T2}^2 X_d Z_0}\right) \\ X_d = \omega L_s - \frac{1}{\omega C_d} \\ C_d = \frac{C_{J0}}{\left(1 + \frac{V_R}{V_J}\right)^M} + C_P \end{cases} \qquad (28)$$

Derivative $\angle S_{21}$ in VR:

$$\frac{d\angle S_{21}}{dV_R} = \frac{2Z_{T1}^2 Z_{T2}^2 Z_0 M C_{J0}\left(X_d^2 + Z_{T2}^2\right)}{\omega V_J C_d^2 \left(1 + \frac{V_R}{V_J}\right)^{M+1}\left[Z_{T2}^4 Z_0^2 X_d^2 + Z_{T1}^4\left(X_d^2 - Z_{T2}^2\right)^2\right]} \qquad (29)$$

where ω, V_J, C_d, Z_{T2}, M, C_{J0}, Z_0, L_s, C_P are known, Z_{T1} is unknown, and V_R and $\angle S_{21}$ are variables.

From expression (27), to see the effect of Z_{T1} on the phase shift, different values of Z_{T1} are investigated by MATLAB to find the $\frac{d\angle S_{21}}{dV_R}$ with smallest maximal point. Firstly, Z_{T1} is roughly experimented with different values from 10 to 80 Ω with the spacing of 10 Ω. From results in **Figure 14**, the value of Z_{T1} can be found around 20 Ω.

Because the value of Z_{T1} is found around the value of 20 Ω, the value of Z_{T1} is examined at a narrower range from 15 to 22 Ω with the spacing of 1 Ω (**Figure 15**).

Among the surveyed values of Z_{T1}, the value of 19 Ω gives the best result and that is the best-chosen value. Thus, the RTPS will be implemented with the load topology, where the impedance of the two microstrip circuits is Z_{T1} = 19 Ω and Z_{T2} = 15 Ω, respectively. The varactors are Skyworks SMV1247 with capacitance from 8.5 to 0.7 pF corresponding to bias voltage from 0 to 5 V.

3.2.3 Direct current (DC) feed and DC block

As mentioned above, varactors are the elements in microwave circuit, and their capacitance value is controlled by a DC bias from controllers. With respect to the
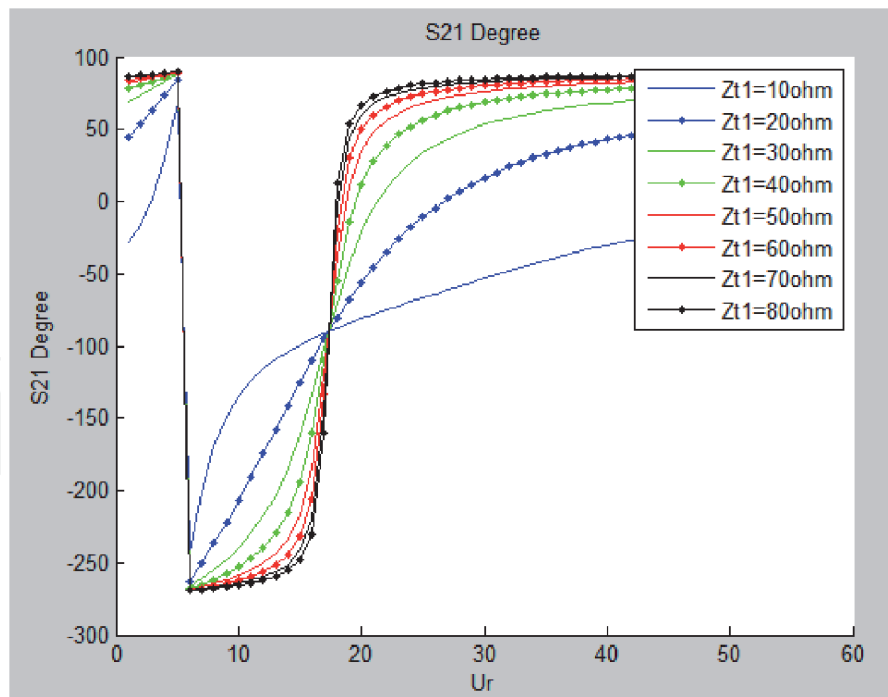
a)
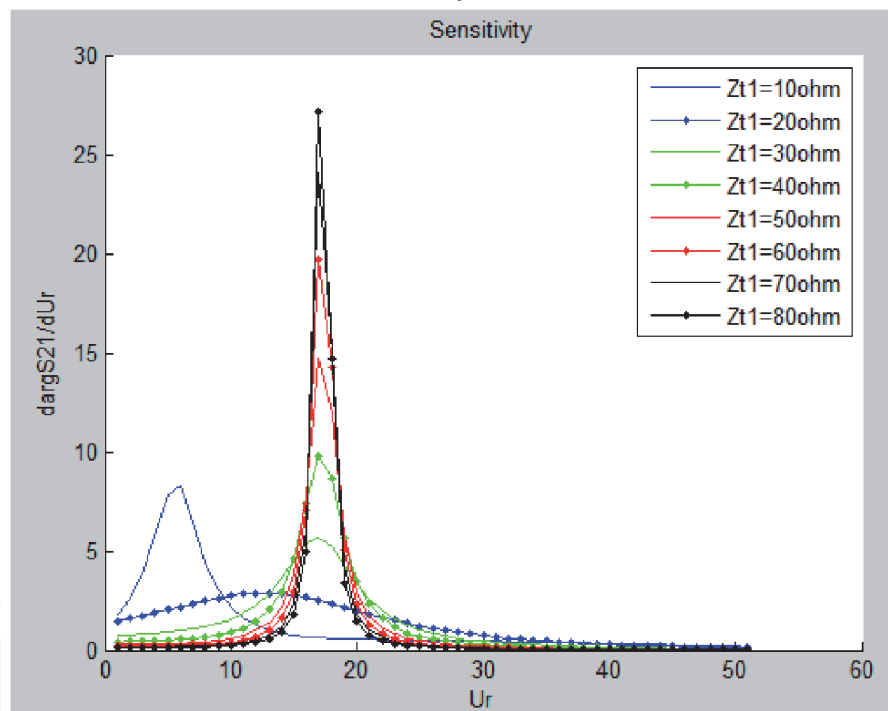
(b)

Figure 14.
The results from the first survey of Z_{T_1} value: (a) phase shift, (b) $\frac{d \angle S_{21}}{dV_R}$.

principle of microwave circuit, the varactors directly connect to transmission lines.
From controller perspective, the DC bias is put to at two polar, anode and cathode,
of varactors. Therefore, it is easily found that the microwave circuit and the con-
troller are physically connected to each other, which leads to that high frequency
waves can propagate to controller, and DC current can go to microwave circuit.
When propagating to controller, controller can be considered as a new part in
microwave circuit, so characteristics of our design might change unpredictably.
For microwave circuit with reference impedance of 50 Ω, the maximal DC bias for
varactors is 20 V, is corresponding to the power of approximately +36 dBm. This
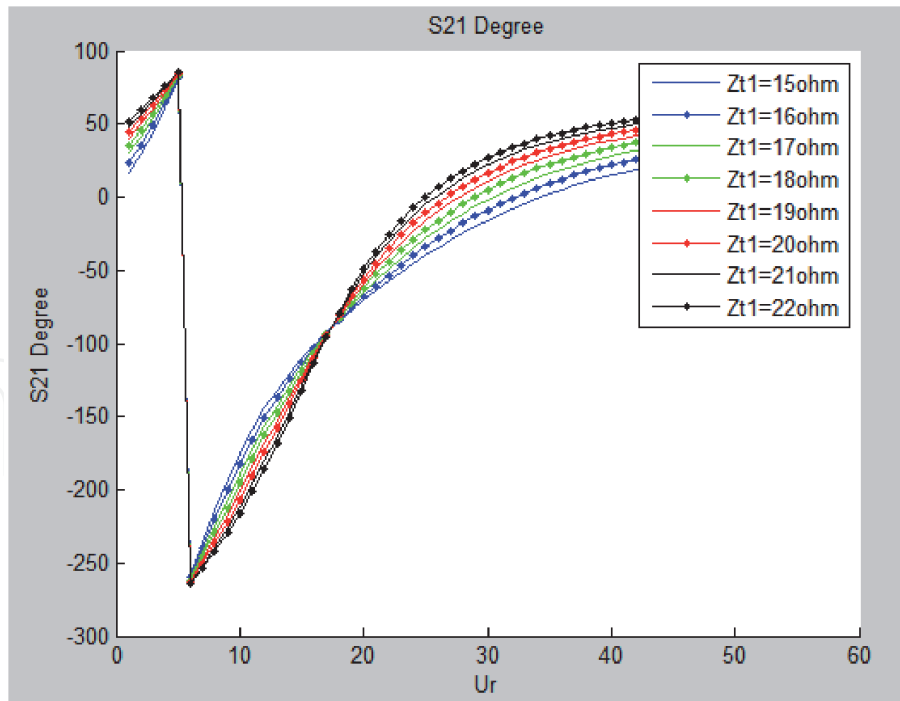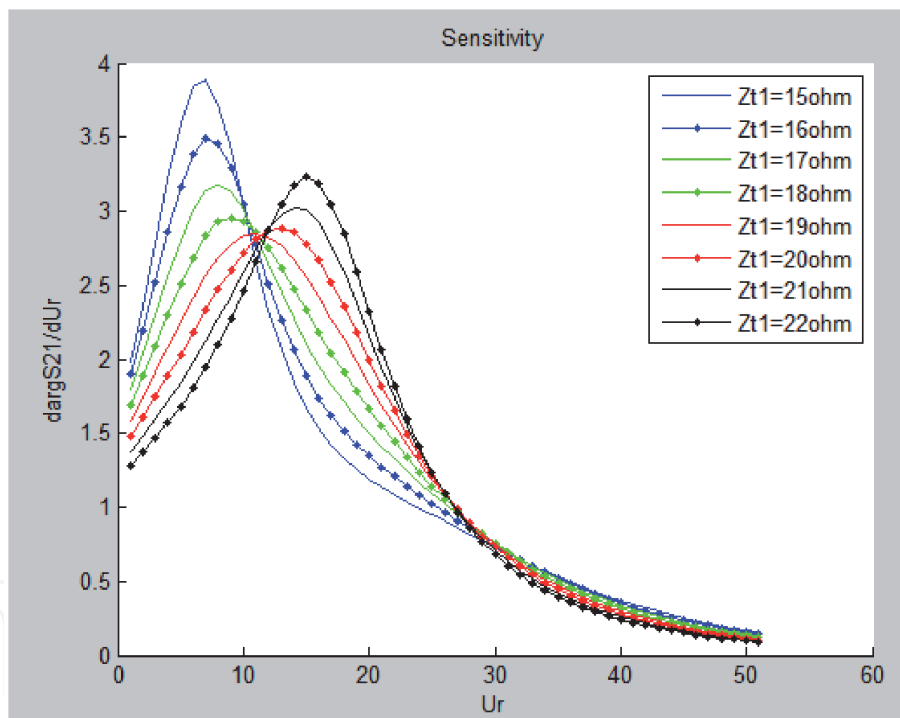
Figure 15.
The results from the second survey of Z_{T_1} value: (a) phase shift; (b) $\frac{d\angle S_{21}}{dV_R}$.

value may exceed the limitation of microwave equipment and instrumentation and can damage them. From these problems, the demand for isolation between microwave and DC current appears. The common solution is to use DC Feed and DC Block components.

DC Block is usually a capacitor, which prevents DC current, but permits microwave circuit to pass easily. The impedance of DC Block must be very low ($<5\,\Omega$) compared with reference impedance ($50\,\Omega$) at operating frequencies (2.45 GHz). To deploy capacitors on microstrip, gap and microstrip interdigital capacitors may be options. However, with impedance less than $5\,\Omega$, the capacitance must be larger

than 13.2 pF at 2.45GHz. That capacitance value is hard to be met by gaps or microstrip interdigital capacitors. For capacitor components, in practice, at microwave frequency, a capacitor component is equivalent to a series of inductor, resistor, and capacitor, so the impedance of DC Block changes in frequency. Above a certain frequency threshold, that DC Block will act as an inductor. Thus, DC Blocks are usually capacitors with its self-resonant frequency near operating frequency, 2.45 GHz. Finally, the DC Block is VJ0603D8R2CXP capacitor of Vishay/Vitramon with impedance about 3.8 Ω at 2.45 GHz, as shown in **Figure 16**.

In contrast, the DC feed is usually an inductive element, which blocks high frequency waves and passes DC current. The impedance of DC Feed element must be very high compared with the reference impedance (50 Ω) at operating frequency, 2.45 GHz. Similar to DC Block, the DC Feed may be an inductance element with a self-resonant frequency near 2.45 GHz operating frequency. However, in practice, due to cost constraint and the availability of inductors, these inductors are replaced by another option, taking advantage of some special case in length of transmission lines. To minimize the whole structure, the quarter-wavelength transmission line used is shorted at the end, of which the equivalent impedance is positive infinity at operating frequency. In other words, a quarter-wavelength transmission line with shorted at the end can be treated as an open circuit at the beginning of that transmission line. Consequently, the DC bias can be replaced at the end of quarter-wavelength transmission line, so that high frequency waves do not reach the DC circuit while the DC currents can flow directly to varactors.

There exist two ways to short a circuit. The first way is to use via holes to create physical connection from electric lines to the ground; however, this method also shorts the DC bias. The other way is to employ open quarter-wavelength straight stubs or radial stubs. These two kinds of stubs do not physically connect to the ground, so they do not short the DC bias. In [28], Gardner and Wickert mentioned that radial stubs, possibly realized as shunt stubs with low characteristic impedance, may avoid the problems of transverse resonance and poorly defined point of attachment associated with straight stubs. In our DC Feed, the radial stubs are the suitable choice. Some research groups have studied about the equations for the formulation of microstrip radial stubs [27, 29–31]. Based on these studies combined with optimization tool in Advanced Design System software, the optimized
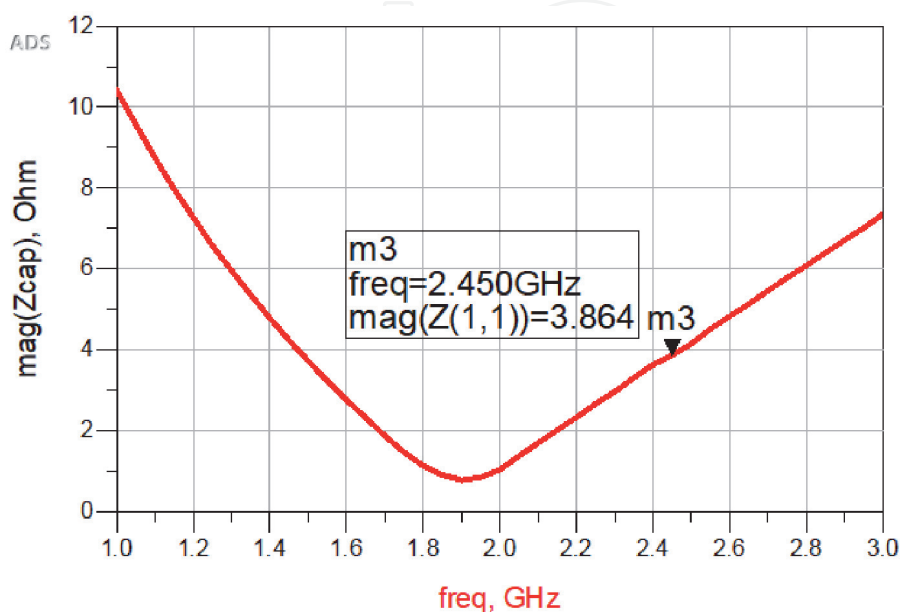

Figure 16.
Impedance of DC block VJ0603D8R2CXP.

parameters calculated for the Roger4003c substrate radial stubs are: the outer radius R_o = 540.621 mil and the inner radius R_i = 56.688 mil and angle α = 30°.

3.2.4 Design of controller for reflection type phase shifter

In phase array antennas, in order to be able to steer the antenna's main lobe in different directions, the phase-shift system must be placed in front of the antenna elements to generate the phase difference of the wave to each antenna so as to create the angle of beam. The phase shift entirely depends on the capacitance value of the varactors whereas every varactor always has its own C – V characteristic curve, representing the relationship between the input applied voltage and output capacitance. In other words, the phase shift is controlled by the voltage applied to the anode and cathode pins of varactors. For SMV1247 varactor, the voltage range of 0–5 V is applied. Thus, the controller is required to generate adjustable voltage in the range of 0–5 V, providing eight different voltages for eight RTPS and each voltage channel must meet the total power of four varactors in a RTPS.

To generate a DC voltage controlled by the microcontroller, popular methods are to modulate pulse width or control open angle of power semiconductor components such as Triac or Thysistor to convert AC to DC. These two methods are commonly used in power circuits, so we usually only care about the average power and voltage in a cycle, but in essence, the voltage generated is not flat over time but it is ripple. Obviously, these two methods will not be able to generate the control voltage for the varactors, which constantly changes the capacitance and results in undesired phase shifts. From the datasheet of SMV1247 varactor, the reverse current is very small, just a few nA to μA, so it is possible to use Digital to Analog Converter (DAC) units. Output current of these elements is about 20 mA. It is enough to satisfy the reverse currents of four varactors in a RTPS. In addition, the DACs have a variety of resolution options ranging from 8 bits to 24 bits. This facilitates flexible adjustment of the RTPS resolution. Therefore, the controller will be designed based on the eight DAC elements to generate bias voltages for eight RTPS. The controller model is described in **Figure 17**. The main components are DACs, and in order to increase the accuracy of the output voltage, the DACs are powered by a different source with a higher accuracy than the source for the microcontroller or can be adjusted for backup case when higher voltage range of varactors is demanded.

3.2.5 Design of antenna element

Because the positioning system is executed indoor, the WiFi or Wireless LAN should be the most suitable protocol to use in order to radiate power to indoor mobile devices; therefore the 2.4 GHz to 2.484 bands is chosen as the operating frequency. On the other hand, in order to communicate with the mobile devices for localizing the position of the object, the angel of main beam of phased array antenna should change from −45 to 45° to scan the desired object, hence antenna element must have half power beam width [15] greater than 90°. These requirements demonstrate that the radio signal strength comparison completely depends on the array factor. Omnidirectional antennas can satisfy both requirements; however, some omnidirectional antennas such as dipoles, ... [15] still have some undesired effects, that is, radiating to the back side of the antenna array, which results in some high side back lobes due to the reflection. The microstrip patch antenna can both meet the above condition and have small back lobes. In our array, the microstrip patch antenna was designed to operate at Wi-Fi band frequency, 2.4 to 2.484 GHz with an input impedance of 50 Ω using a low cost FR4 substrate with dielectric constant ε = 4.3, loss tangent tanδ = 0.02 and thickness h = 62 mil = 1.58 mm. The antenna
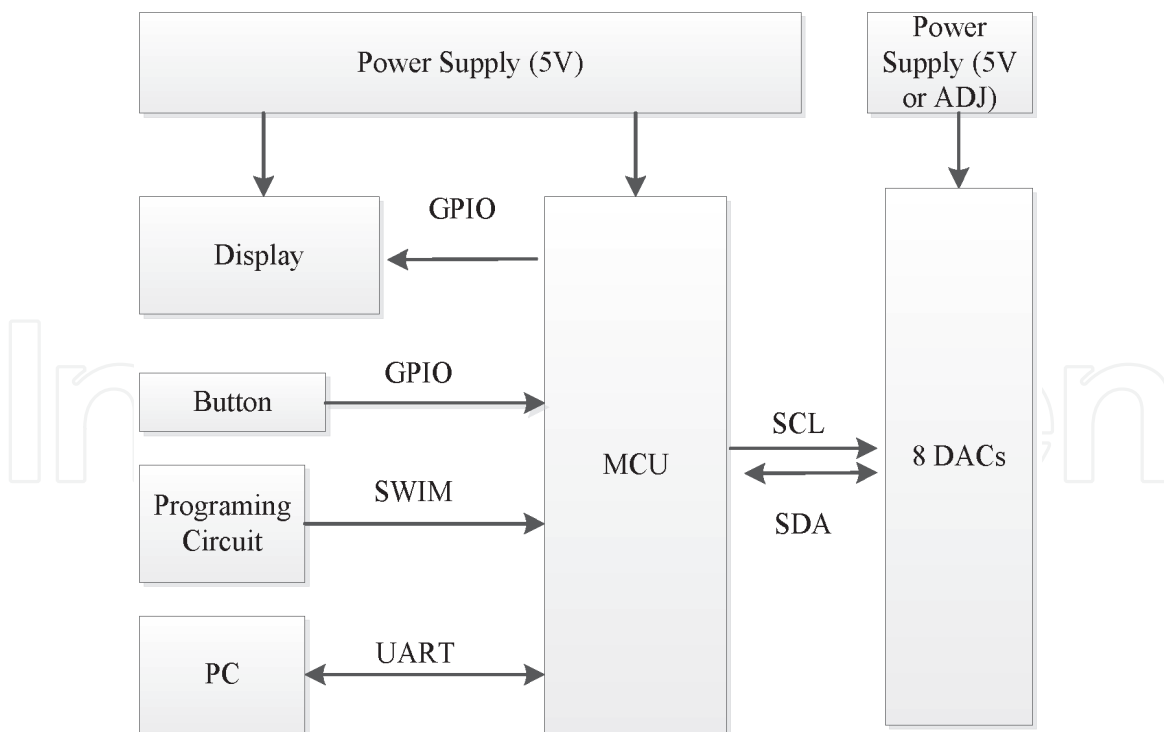
Figure 17.
Block diagram of varactor diode controller.

width W and length L are computed with the following Equation [15, 32, 33] where f is center frequency (2.45 GHz):

$$W = \frac{3 \times 10^{11}}{2 \times f} \sqrt{\frac{2}{\varepsilon + 1}} = 36.60 \; mm \tag{30}$$

$$L = L_{eff} - 2 \times \Delta L = 28.07 \; mm \tag{31}$$

$$\text{where} \begin{cases} L_{eff} = \dfrac{3 \times 10^{11}}{2 \times f \times \sqrt{\varepsilon_{eff}}} = 29.53 \; mm \\[2em] \Delta L = 0.412 \times h \times \dfrac{\varepsilon_{eff} + 0.3}{\varepsilon_{eff} - 0.258} \times \dfrac{\dfrac{W}{h} + 0.264}{\dfrac{W}{h} + 0.8} = 0.73 \; mm \\[2em] \varepsilon_{eff} = \dfrac{\varepsilon + 1}{2} + \dfrac{\varepsilon - 1}{2} \left[1 + 12 \dfrac{h}{W} \right]^{-\frac{1}{2}} = 3.9953 \end{cases}$$

with L_{eff} is the effective length, ΔL is the length adjustment, ε_{eff} is the effective permittivity, and h is the substrate thickness.

4. Evaluation of phased array antenna performance

To validate the design of the antenna, every component in the phased array structure is evaluated and measured. All the simulations are performed on Keysight Technologies's Advanced Design System (ADS) software and CST Microwave Studio. All the components are fabricated on the FR4 substrate with dielectric constant ε of 4.3, loss tangent tanδ of 0.02, substrate thickness h of 62 mil (1.58 mm), and the conductive copper thickness t of 1.4 mil (1 oz).

4.1 Array component design and evaluation

4.1.1 Wilkinson power divider (WPD)

In the two-way WPD, theoretically, the total input power is equally divided into two output ports. Assume that the input port is port 1 and the output ports are port 2 and 3, the transmission coefficient S21 = S31 = − 3dB as shown in **Figure 18b**.

However, microstrip circuits on any substrate are affected by the loss tangent coefficient of the substrate and the microstrip discontinuities. The loss tangent represents the loss in the dielectric. The higher the loss tangent is, the more the loss is. For FR4 substrate, the loss tangent is about 0.025, so the forward gain of WPD on FR4 is less than theoretical one. Furthermore, the microstrip discontinuity phenomenon, as well as [22, 34, 35], appears in practice and generates parasitic

a)

b)
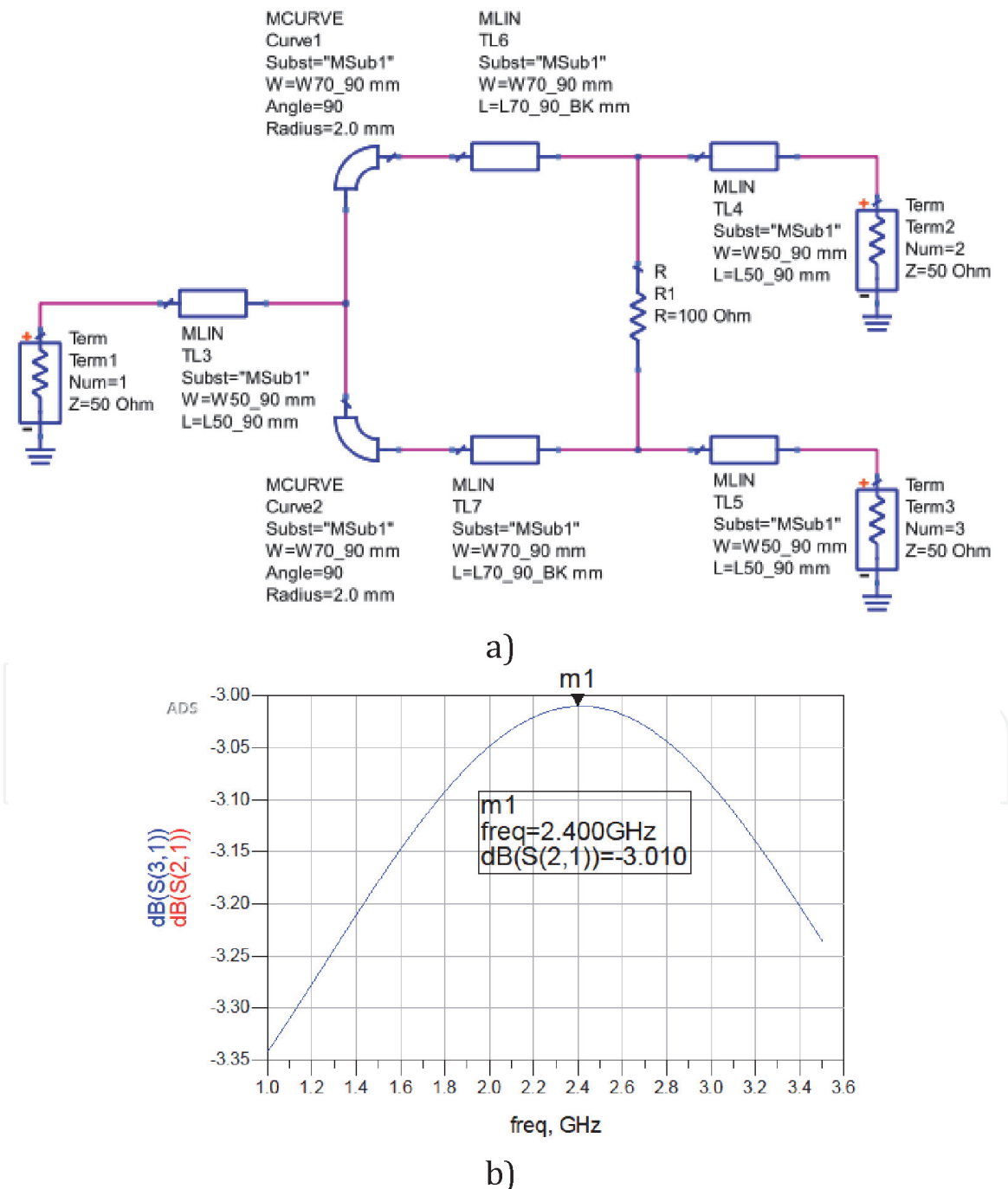
Figure 18.
The simulated 2-way WPD: (a) schematic circuit; (b) forward gains S_{21}, S_{31}.

components, changing the parameters of circuit. Thus, in simulation, it is necessary to insert discontinuity components such as Bend and Tee so that the simulated results are close to measured results. After that, dimension of transmission lines is slightly adjusted by using optimization tool in ADS software in order to get the desired results. The two-way WPD is shown in **Figure 19** and $S_{21} = S_{31} = -3.23$ dB.
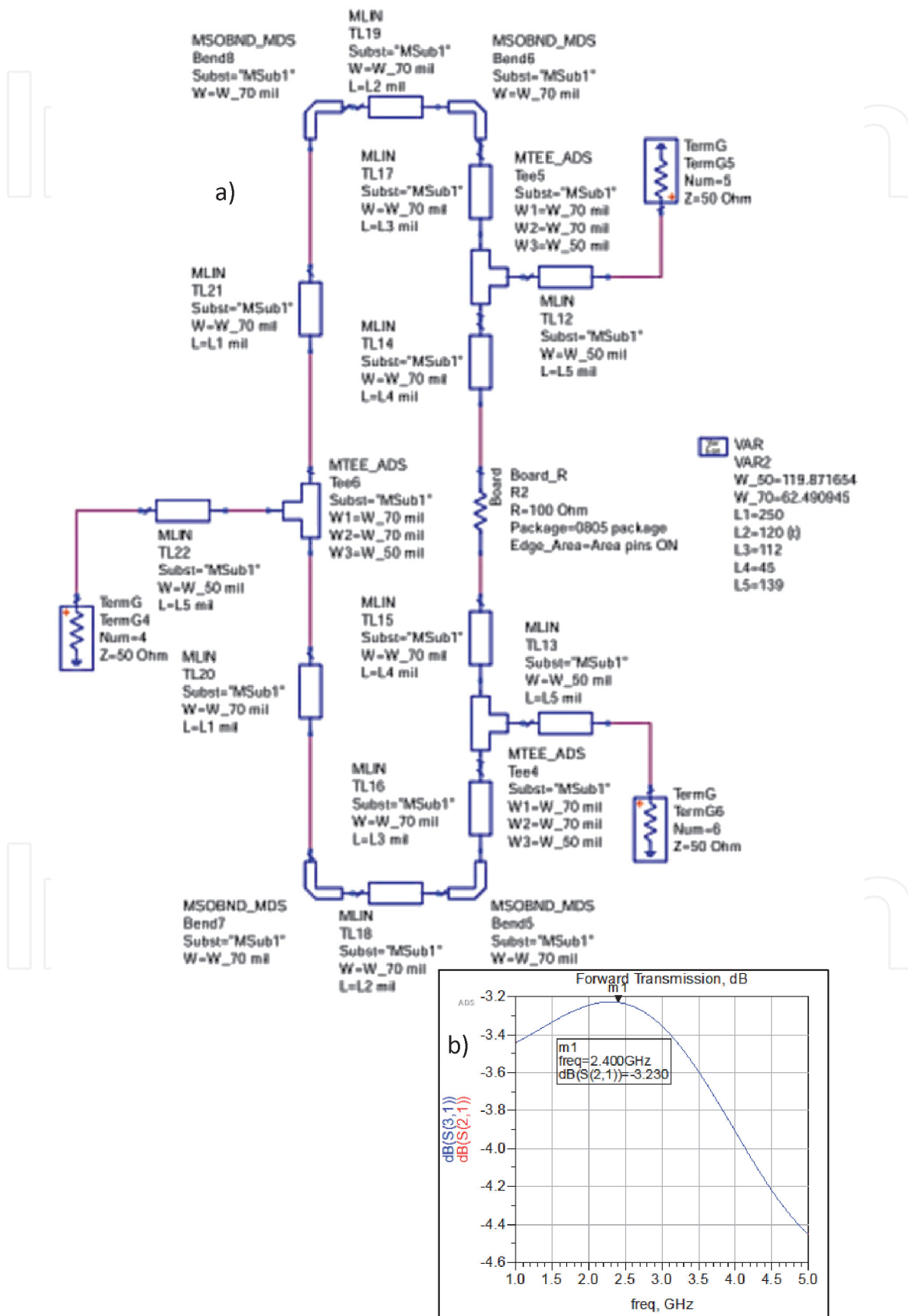
Figure 19.
The 2-way WPD: (a) schematic circuit; (b) forward gains S_{21}, S_{31}.

According to the cascade structure, the eight-way WPD is formed from the two-way WPDs and 50 Ω transmission lines. In addition, in microwave circuit, when transmission lines are placed closely to each other, the coupling between them occurs, which affects to characteristics of circuit. The coupling is an issue not easy to calculate and estimate and does not appear on schematic simulation, so the EM simulation and EM co-simulation are used to ensure the final simulated results (**Figure 20**).

Finally, the eight-way WPD is fabricated on FR4 substrate and then measured by PNA N5222A network analyzer. The forward gain for each port are shown in **Figure 21,** in which the thin red line, bold blue lines, and blue dash lines are forward gains of 8-way WPD in schematic simulation, EM co-simulation and fabrication, respectively. It can be seen that for schematic simulation, the forward gains in all output ports are identical and equal to −10.882 dB instead of −9 dB as in theory. The loss occurs during propagating on FR4 substrate with loss tangent coefficient tanδ = 0.025. For EM co-simulation, the forward gains at the output ports are not identical and change from −11.031 to −10.493 dB. As mentioned above, the difference comes from the coupling between transmission lines.

The forward gains of 8-way WPD made on FR4 material are relatively close to the simulation results in the schematic circuit and EM co-simulation at the designed frequency 2.45 GHz. The measurement results change around the simulation results with a difference less than 1 dB. The differences are due to the fabrication tolerance as well as the heterogeneity of the material in reality, causing the change of mismatch and loss compared with simulation. For the other frequency band, namely less than 2.4 GHz and greater than 2.5 GHz, there are large differences between simulation and reality. The reason is that the fabrication errors will make a great impact at undesired frequencies. However, this error does not affect the final result because the system is designed to operate at 2.45 GHz.

Additionally, in **Figure 22,** the thin red line, thick blue line and dash blue line represent the schematic simulated result, electromagnetic co-simulation, and the measured result, respectively. The isolation between output ports of the power divider is about 20 dB, similar to products on the market.

4.1.2 Reflection type phase shifter

For low loss variation, the important component – RTPS is designed on substrate Roger4003C with dielectric constant ε of 3.55, loss tangent tanδ of 0.0021 and substrate thickness h of 0.8 mm. The RTPS structure is simulated on Advanced Design Systems ADS software. ADS has built-in components such as microstrip lines, terminals, DC voltage, and stubs; however, the selected SMV1247 varactors are not supported, hence it is necessary to create an equivalent model of SMV1247 before designing and simulating the RTPS. The C-V characteristic curve of SMV1247 with the ADS model at 100 MHz is shown in **Figure 23b**. This curve is
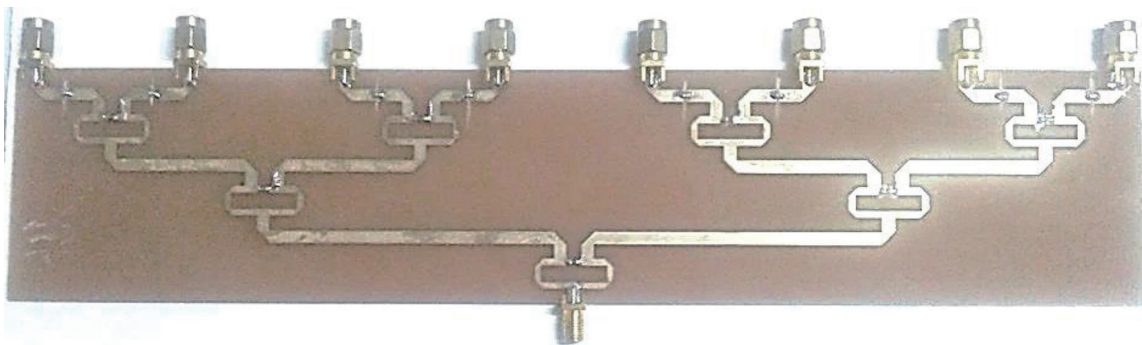

Figure 20.
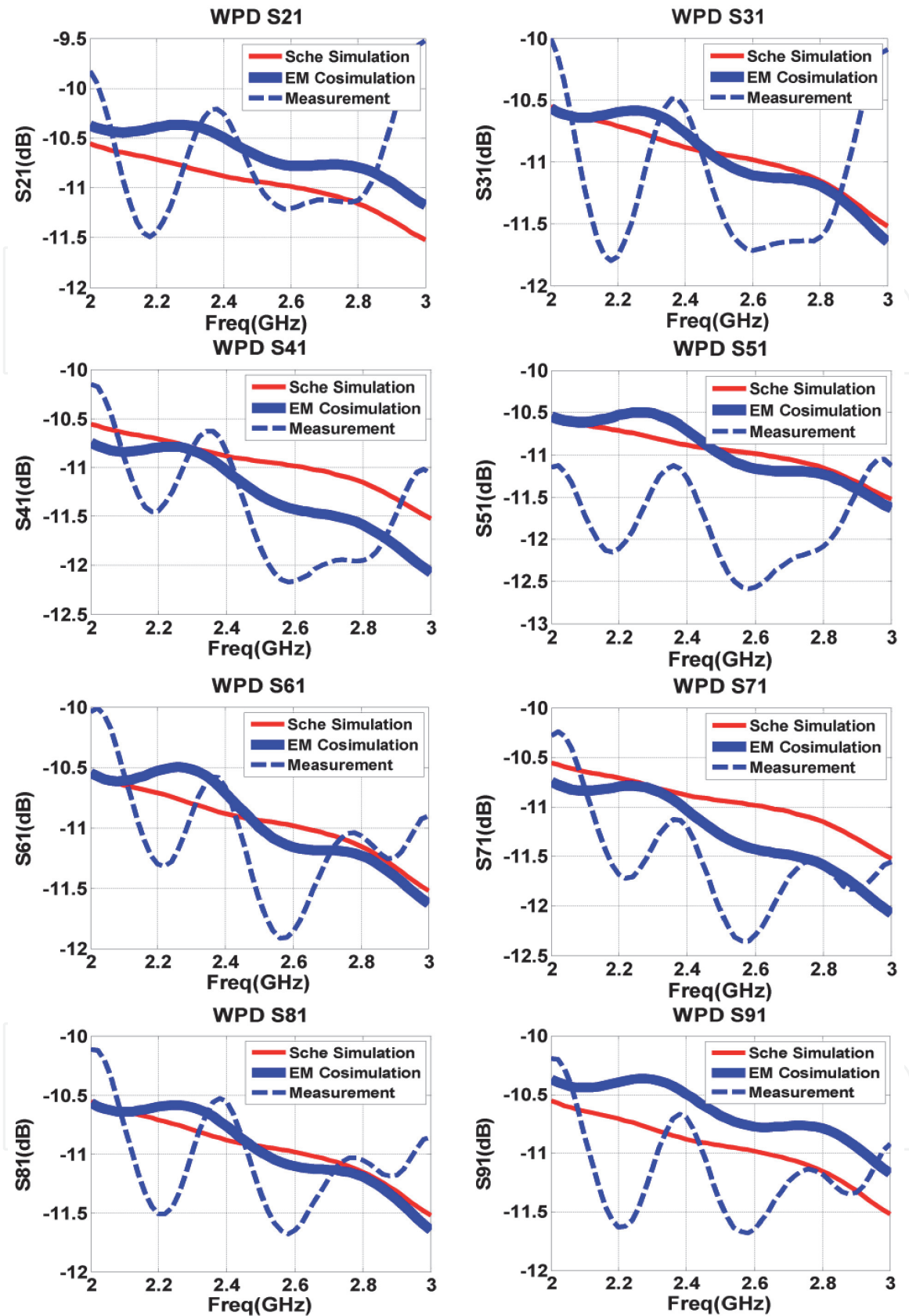*Eight-way Wilkinson power divider.*

Figure 21.
Forward gain from port 2–9 of the WPD.

similar to the characteristic curve in the SMV1247 datasheet **Figure 23a**, so this SMV1247 model will be used on all ADS simulations. These characteristic curves were calculated from model in **Figure 24**.

In the technical documentation of SMV1247, Skyworks provides the SPICE model (**Figure 24a**). After importing this model into ADS software, the equivalent
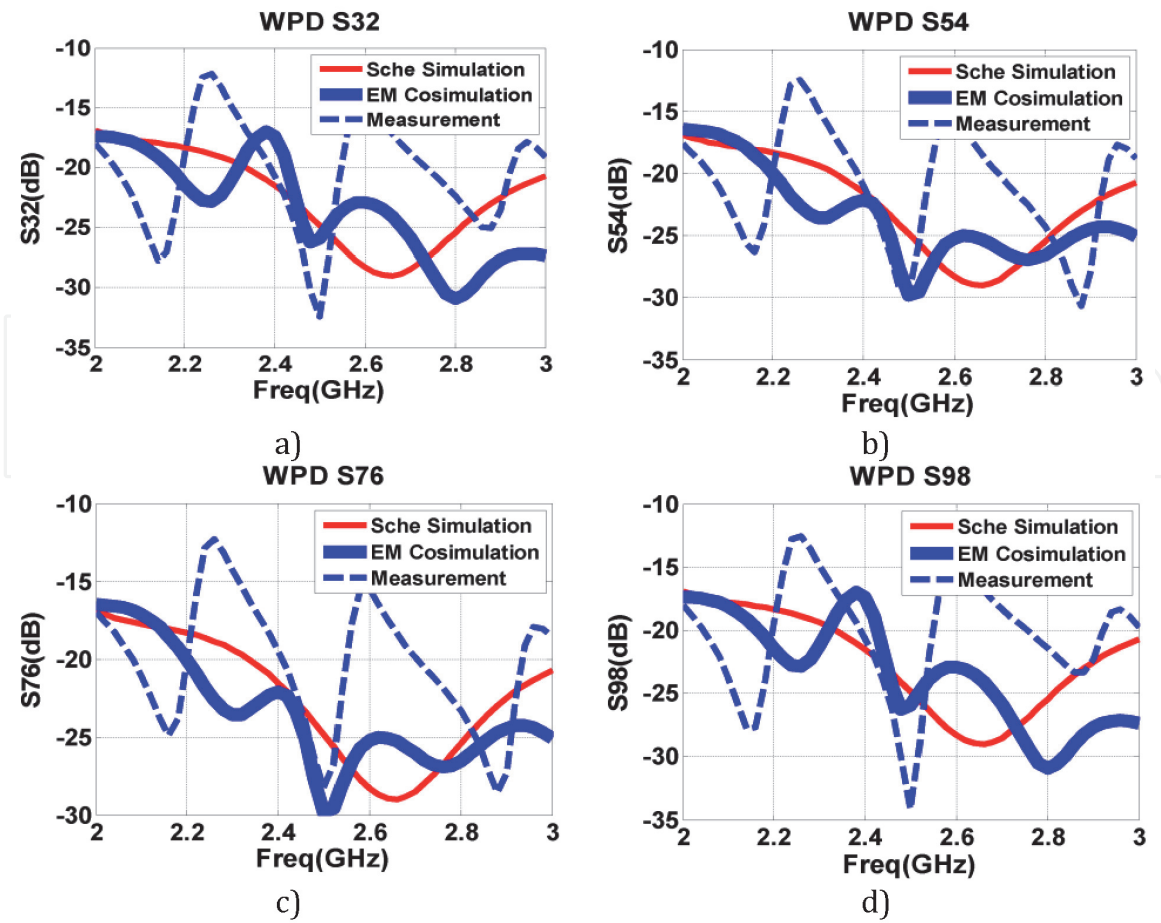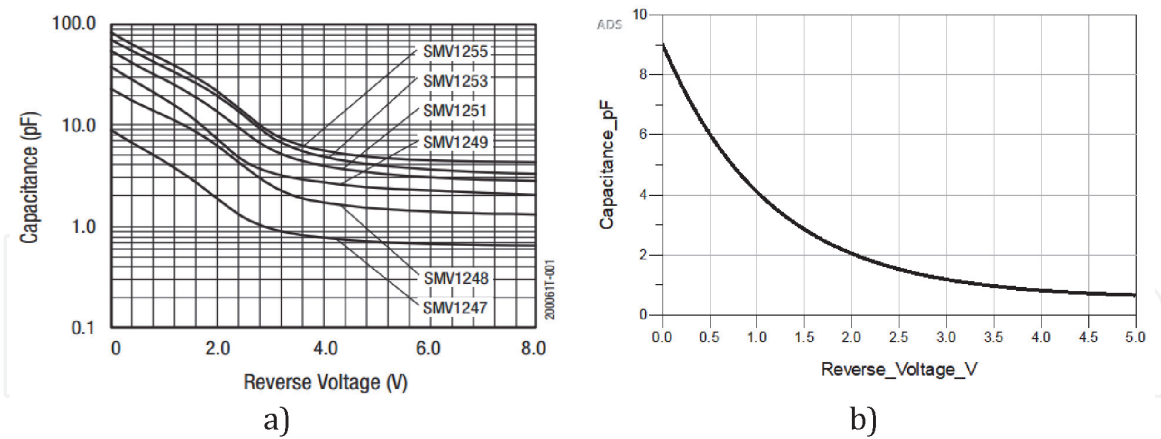
Figure 22.
Isolation between output ports.

Figure 23.
C-V curve of SMV1247 on: (a) technical document [36]; (b) ADS.

model of SMV1247 is built with the L_s, C_p, and R_s values corresponding to SC-79 packages, L_s = 0.7nH, C_p = 0.54 pF, and R_s = 4.9 Ω (**Figure 24b**).

The RTPS is deployed both in schematic simulation and EM co-simulation to ensure the real operation (**Figure 25**). The microstrip discontinuity components such as bend, tee, and steps in width are inserted and their dimensions are adjusted in order to obtain the desired results. Then the RTPS is fabricated on Roger4003c (**Figure 26**) and measured by the Keysight PNA N5222A Network Analyzer.

The results of the phase shifter are shown in **Figure 27**, where the green dash line, blue dash dot line, and red circle line are schematic simulation, EM co-simulation, and measured results, respectively.

a)

b)
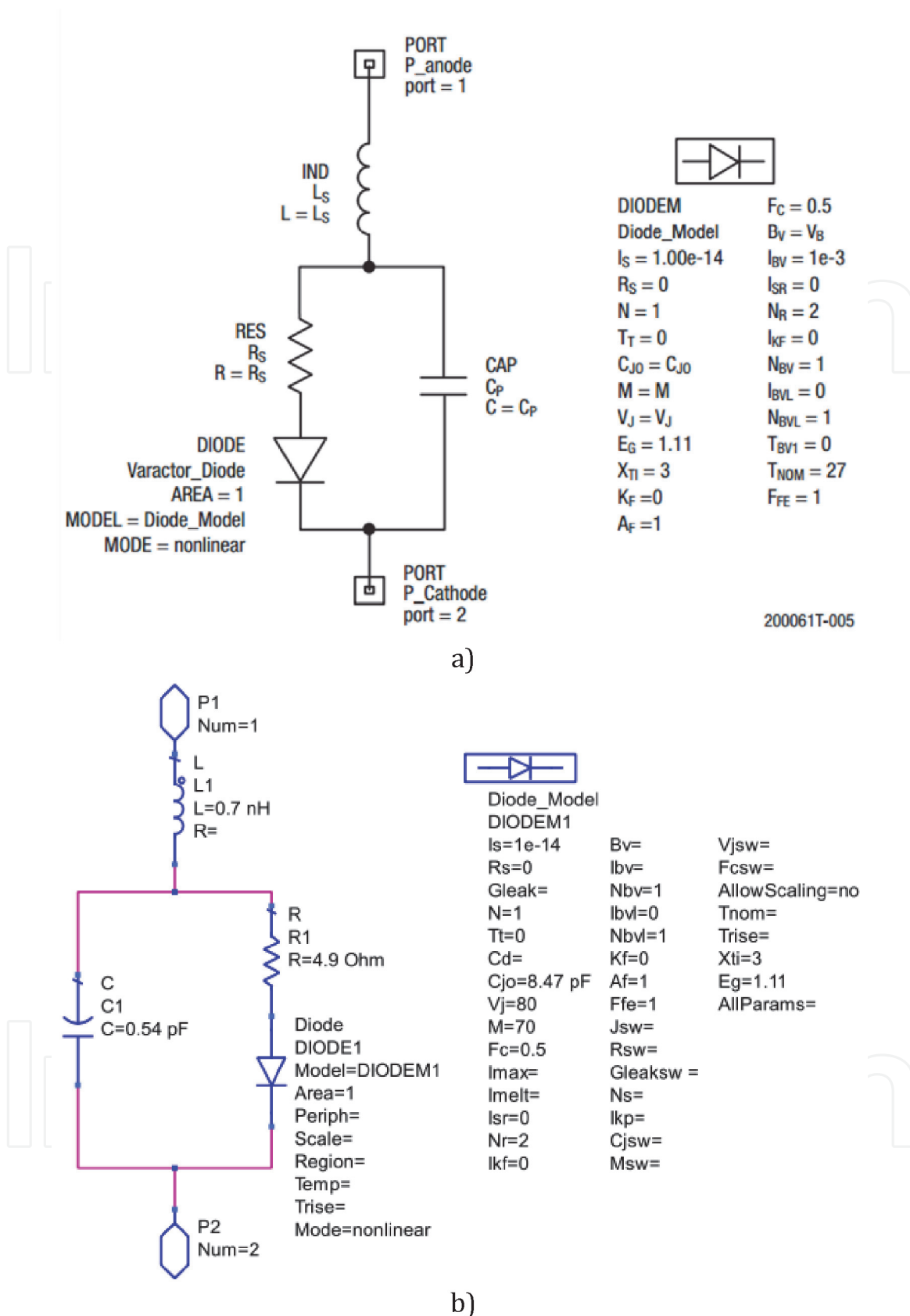
Figure 24.
Equivalent model of SMV1247: (a) on SPICE [36]; (b) on ADS.

Figure 27 shows the forward gains (S_{21}) in all three cases simulating the schematic, electromagnetic field simulation, and measurement results. I find that the energy transmitted through the phase shifter is little less than that of the schematic and electromagnetic simulation. The reason may be due to the error in fabrication process as well as contact between the varactors and the microstrip line, which is
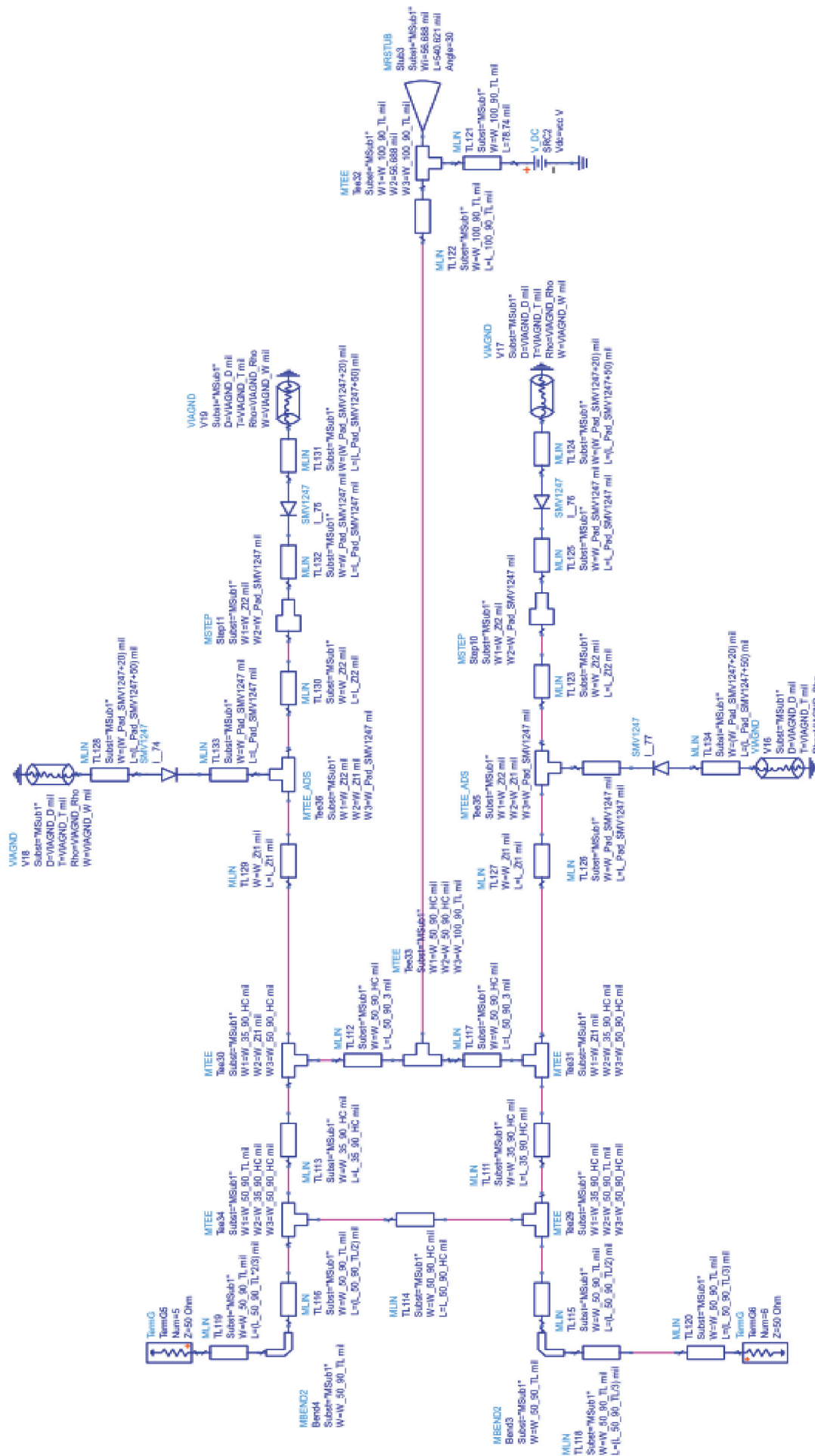
Figure 25.
Schematic circuit of reflection type phase shifter on ADS.
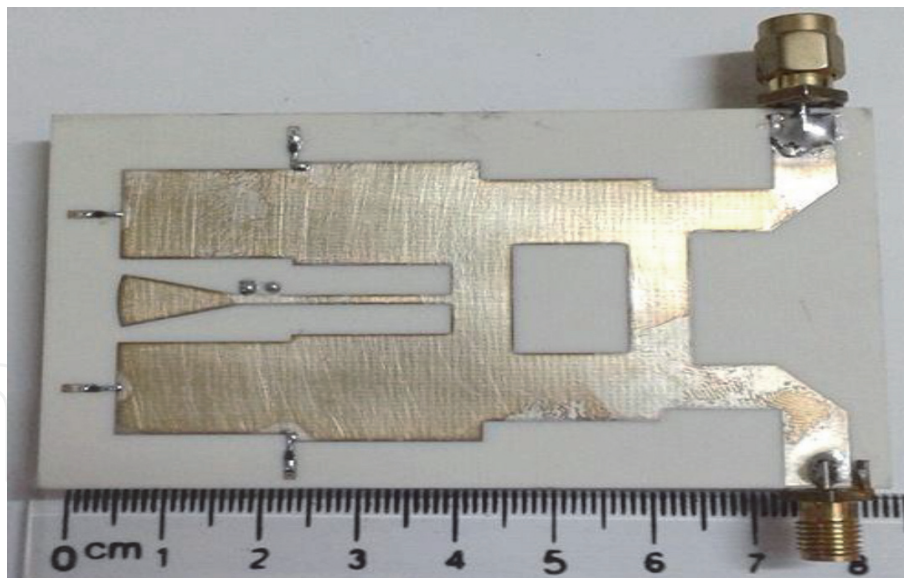
Figure 26.
Reflection type phase shifter fabricated on Roger4003c.

a)   b)
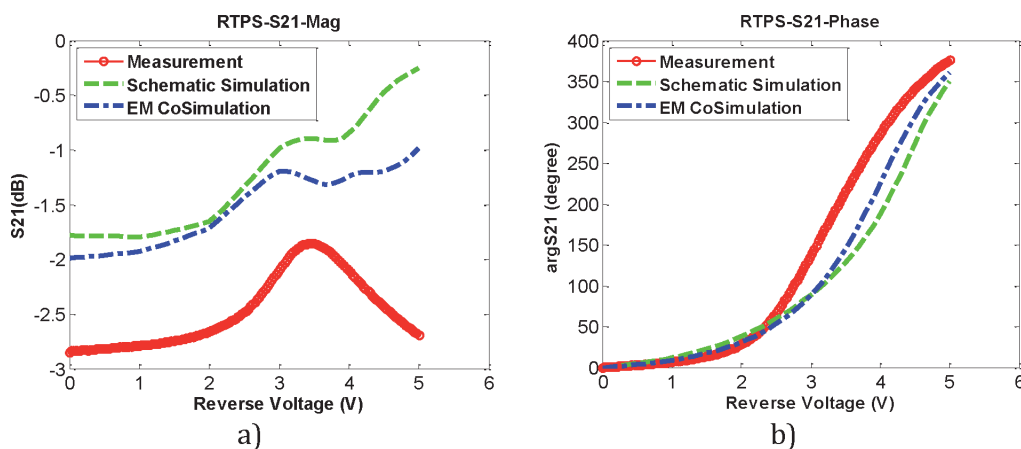
Figure 27.
Transmission coefficient S_{21} of RTPS: (a) magnitude; (b) phase.

not ideal and alter the resistance value in the equivalent circuit of the varactors and resulting in a loss of power that is much larger than simulation. The insertion loss is about 2.5 dB with nearly 0.5 dB of variation. The low insertion loss variation enables us to make a phased array antenna with uniform amplitude and spacing. **Figure 27b** shows phase shifts in three cases, the schematic, electromagnetic simulation, and measurement results. The phase shifters are capable of shifting about 370°. The phase shifter in reality although is not nearly as linear as the rest of the two cases, but with DAC12bits, the phase shifter can still be controlled with small resolution.

4.1.3 Microstrip patch antenna

The fundamental part – microstrip patch antenna is simulated on CST Microwave Studio software and then fabricated on FR4 material, as shown **Figure 28**. In order to determine the bandwidth of an antenna, two parameters, VSWR and return loss S_{11}, can be measured by the network analyzer PNA N5222A. At the operating frequency, the desired VSWR and S_{11} are less than 2 and −10 dB,
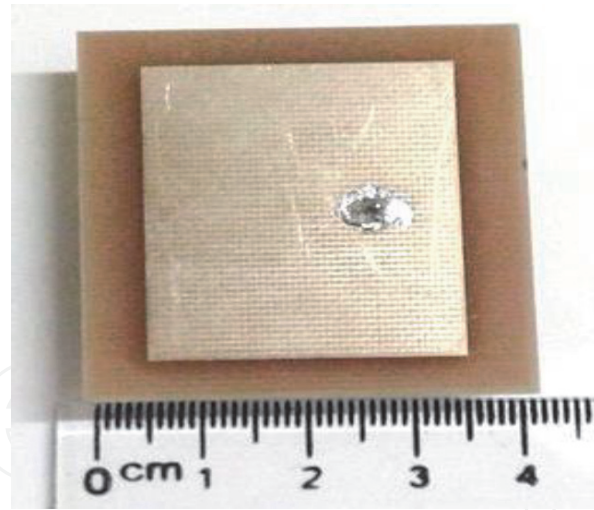
Figure 28.
Fabricated microstrip patch antenna.

respectively. The VSWR and S11 of patch antenna versus frequency are shown in
Figure 29, where the thin red lines and dash blue lines are simulated and measured
characteristics, respectively. It can be seen that in simulation, my microstrip patch
antenna can operate at Wi-Fi band with resonant frequency from 2.4 to 2.484 GHz.
However, due to the heterogeneity of the material in practice as well as errors in
fabrication, my microstrip patch antenna in reality can only operate from 2.424 to
2.485 GHz. Although this antenna cannot be used in whole range of Wi-Fi band, it
can still operate at several channels of Wi-Fi.

(a)

(b)
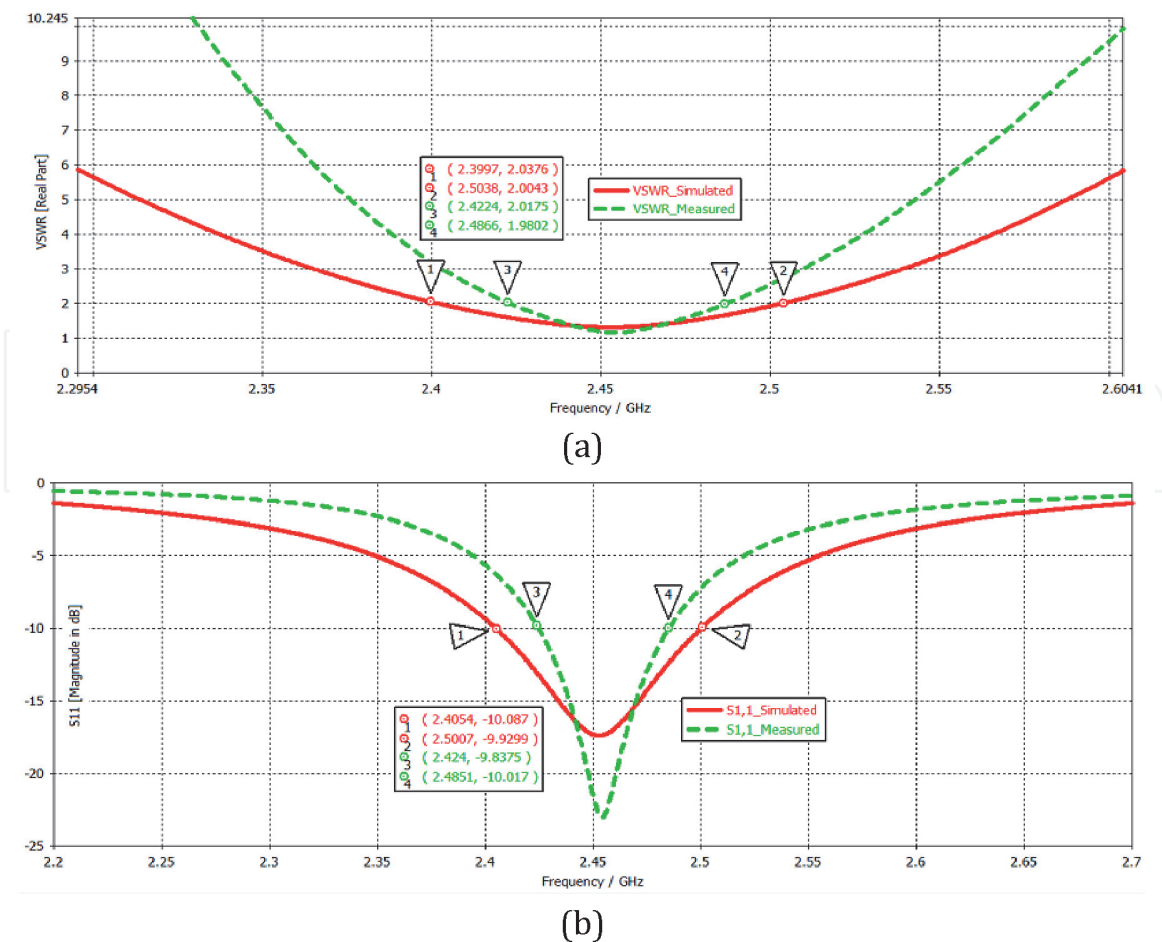
Figure 29.
Microstrip patch antenna parameters: (a) VSWR; (b) return loss.

4.2 Beamforming antenna measurement evaluation

4.2.1 Material and facility preparation

In general, the radiation pattern of an antenna is three-dimensional. Because it is impractical to measure a three-dimensional pattern, a number of two-dimensional patterns are measured. Patterns can be obtained by fixing one of angles (θ or ϕ) while varying the other. For a single antenna, the $\theta = \pi/2$ azimuthal pattern and $\phi = 0$ elevation pattern are usually chosen. For phased array antenna, only $\theta = \pi/2$ azimuthal pattern is measured to observe the direction of main beam, and the $\phi = 0$ elevation pattern does not provide useful information. Ideally, the measurement system would be placed in outdoor space in the far field region to cancel reflection waves. However, this ideal condition is not achievable; therefore indoor anechoic chambers have been developed for this antenna array measurement. The region inside anechoic chambers is covered with RF absorber. The reflection coefficient of anechoic chambers is about -40 dB [15, 37].

Structure of the measurement room is shown in **Figure 30**. A horn antenna, HF 906, is used as a transmitting antenna, and antenna under test (AUT) is received antenna. Thanks to the reciprocity property of antennas, the transmitting and receiving radiation patterns are identical. Therefore, the swap between two antennas is not necessary. The receiving and transmitting powers are measured by the PNA N5222A network analyzer in which the AUT is rotated through a rotating table. To automatically operate this system, a rotating table with an angle step of 5° is set up, and then the measured results are extracted and analyzed from the network analyzer.

Figure 31 shows the radiation pattern of my microstrip patch antenna. We can see that the half power beam width is larger than 90° and the measured radiation pattern is similar to simulated one. Therefore, in terms of radiation pattern, each antenna element meets the requirement for indoor positioning system (**Figure 32**).

4.2.2 Beamforming array measurement

All components of the array including power divider, phase shifter, antenna, and controller are assembled together to form a phased array antenna. The radiation
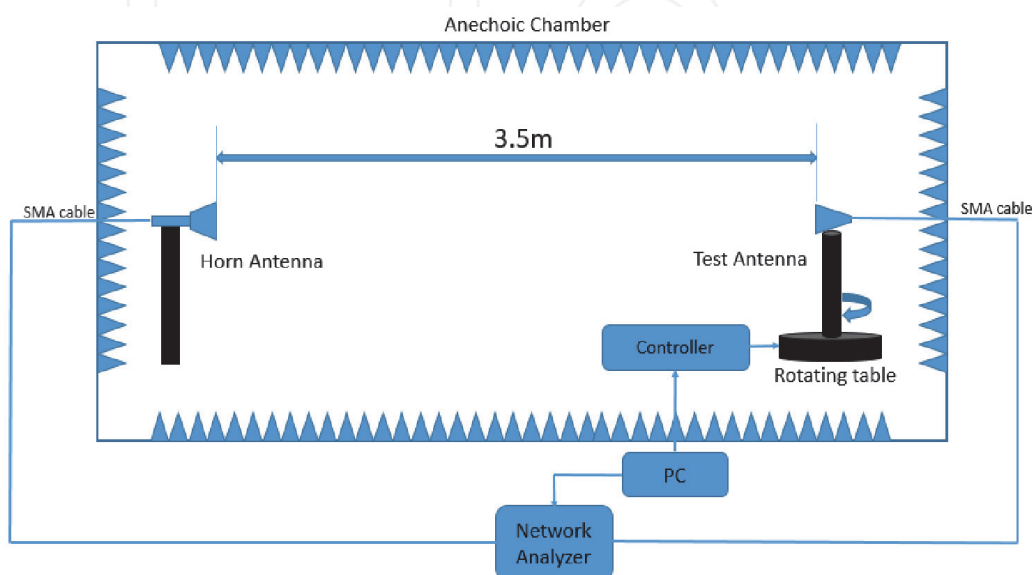
Figure 30.
Anechoic chamber configuration for measuring beamforming antenna array.

Figure 31.
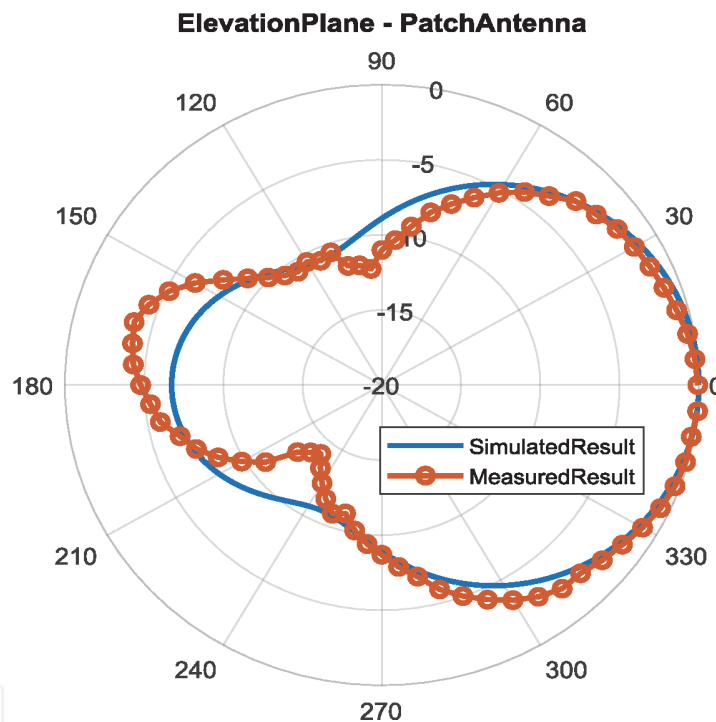*Array antenna measurement in anechoic chamber.*

Figure 32.
*Radiation pattern of microstrip patch antenna element.*

patterns of phased array antenna are also measured in anechoic chamber at General Department of Technical Logistics of the Vietnamese Ministry of Public Security, similar to microstrip patch antenna at 2.45 GHz. The phased array antenna will be mounted in the rotating table to steer the main beam toward angles from −45 to 45° with step of 5°. The measured results are compared with simulated results in same coordinate to investigate the quality of the resulted array (**Figure 33**). The direction of main beam in measurement can track the simulated results. However, when phase shift is tuned, due to variation of electrical length change, and the amplitude variation on both WPD and RTPS causes the difference between direction of main beam in measurement and simulation. Additionally, fabrication tolerance also produces the beam angle error between the measured and calculated value. The measured beam scan angles are within ±5° tolerance (**Table 1**). In general, the measurement results are in good agreement with the simulated results.
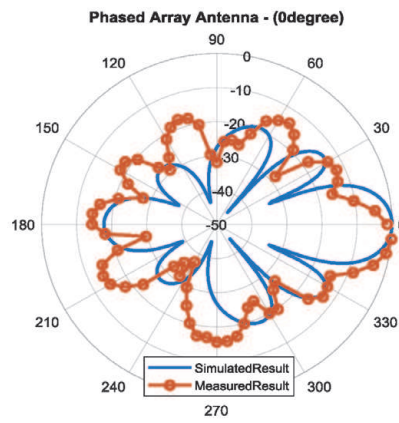
a) Radiation pattern at 0⁰ angle
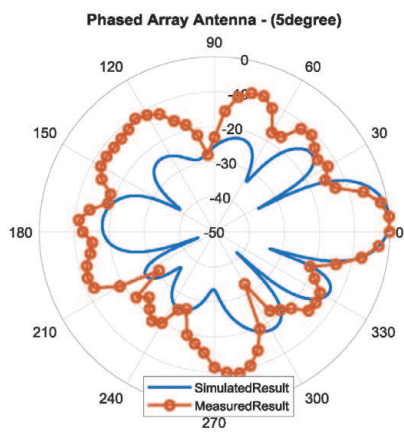
b) Radiation pattern at 5⁰ angle
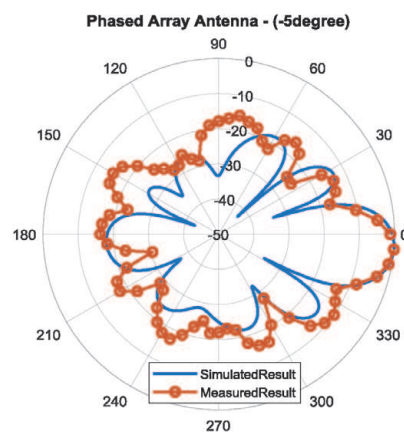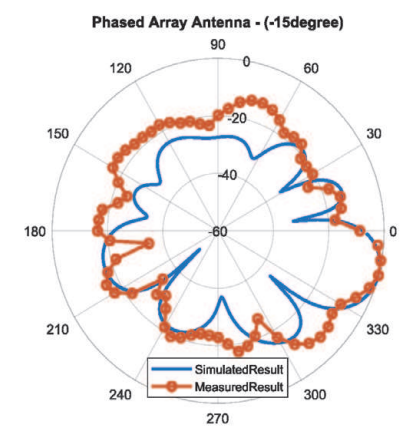
c) Radiation pattern at -5⁰ angle
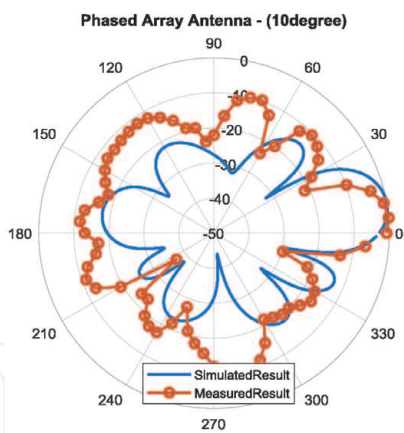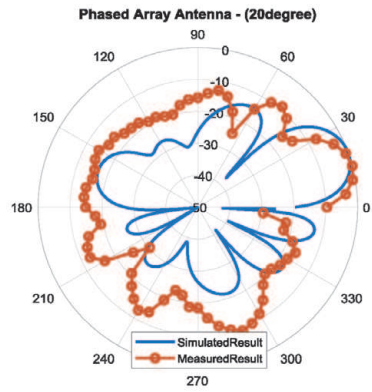
d) Radiation pattern at 10⁰ angle
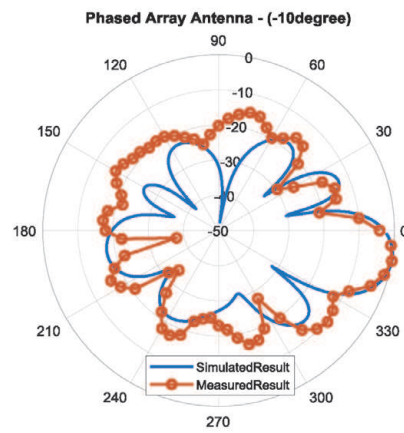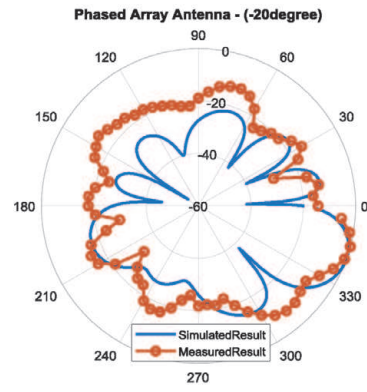
e) Radiation pattern at -10⁰ angle
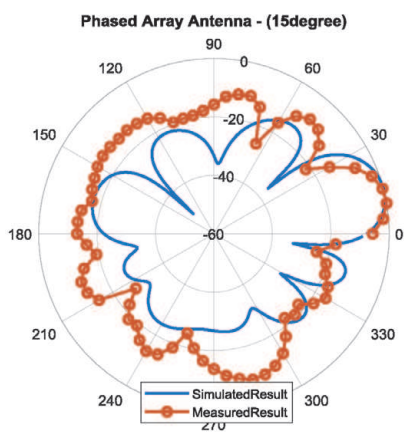
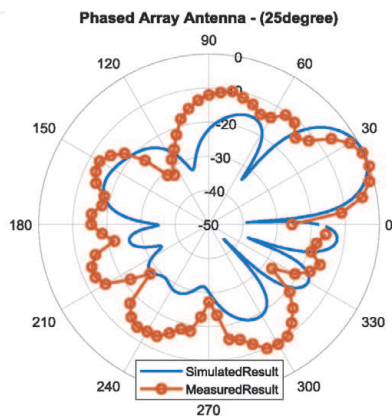f) Radiation pattern at 15⁰ angle

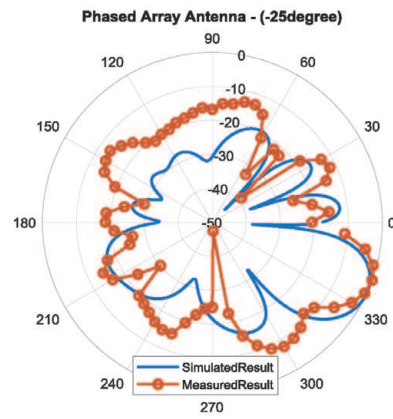g) Radiation pattern at -15⁰ angle
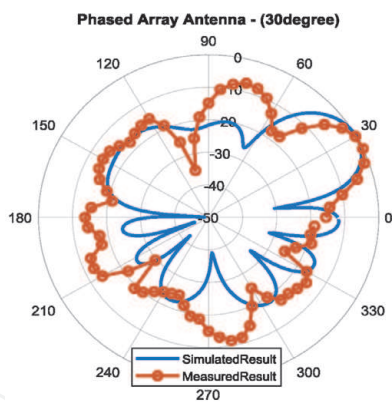
h) Radiation pattern at 20° angle

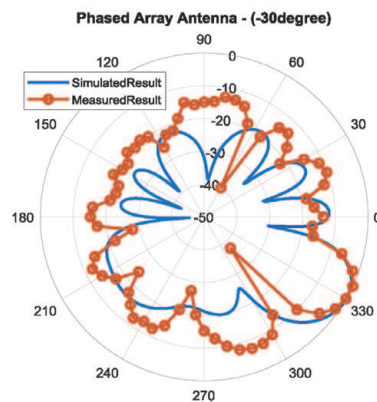i) Radiation pattern at -20° angle

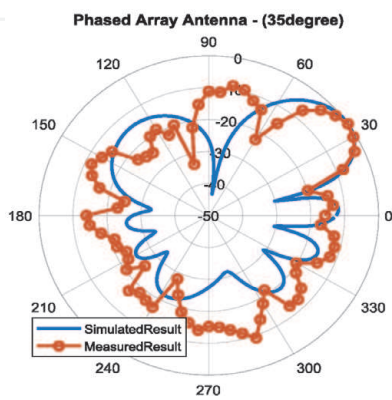j) Radiation pattern at 25° angle

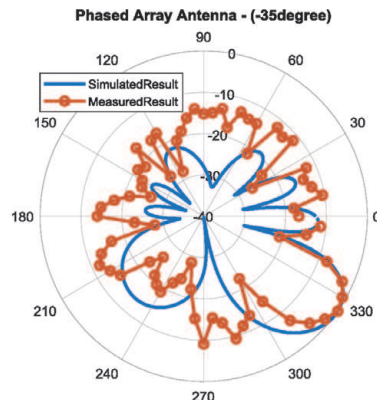k) Radiation pattern at -25° angle
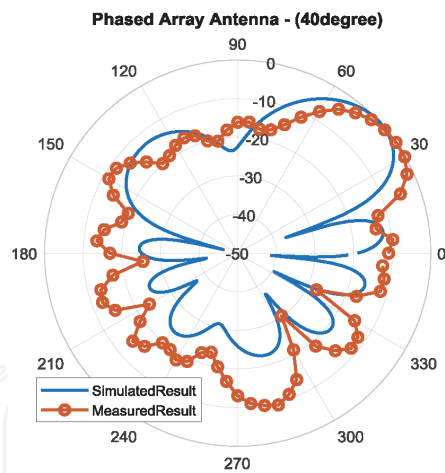
l) Radiation pattern at 30° angle

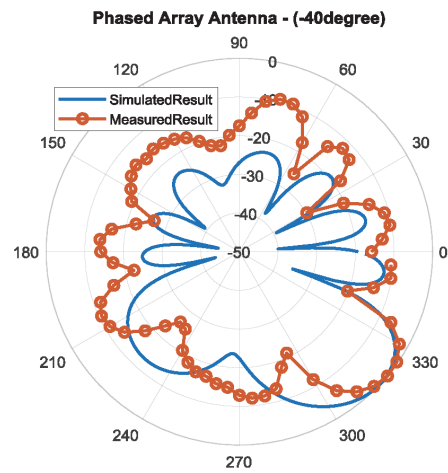m) Radiation pattern at -30° angle

n) Radiation pattern at 35° angle
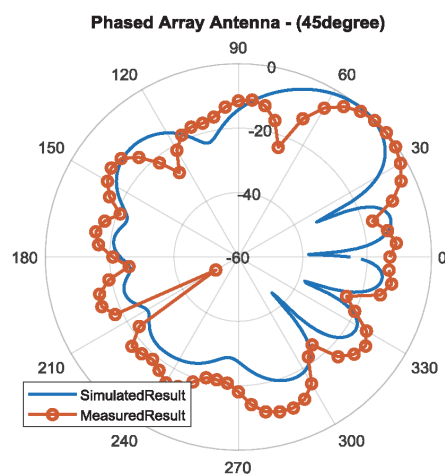
o) Radiation pattern at -35° angle
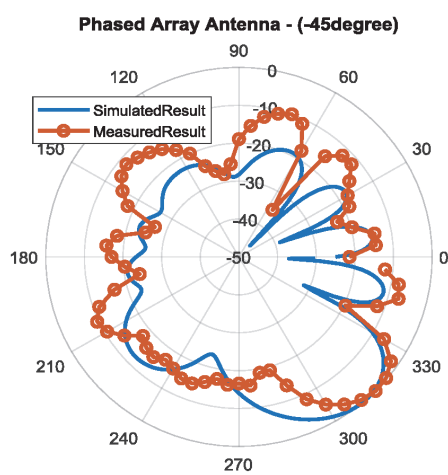
p)   Radiation pattern at 40⁰ angle   q)   Radiation pattern at -40⁰ angle

r)   Radiation pattern at 45⁰ angle   s)   Radiation pattern at -45⁰ angle

Figure 33.
Radiation pattern of phased array antenna at different angles.

Regarding side lobes, compared with simulated results, the gain of side lobes in reality is much higher. The reason is due to the difference of space in simulation and measurement. In simulation, the array antenna is computed in open space, and as a result, there is no affection of reflection on radiation pattern. In reality, although the antenna array is measured in an anechoic chamber, the reflection from wall and other objects in chamber still exist and affect to measured results. Compared with main lobe, side lobe level is less than about 10 dB in most case (**Figure 33**).

A comparison about performance among my antenna design with previous antenna designs for indoor localization is presented in **Table 2**. It can be seen that, in previous designs, based on switching predefined beams, the number of beam is similar to the number of antenna elements. This leads to the limitation of the number of lobes due to the size of an indoor antenna that cannot be too large. Hence, the scan step of these design is quite large, namely 60, 30, 90, and 18° corresponding to researches [10–13]. In this antenna array, by controlling the array factor of array antenna through phase shifter controlling of wave coming to antennas, the number of beam does not depend on the number of antenna element. Simultaneously, the full 360° continuous phase shifter enables me to arbitrarily adjust the phase shift, so the main beam can be steered continuously. The resolution of scanning angle step in steering can be achieved at 5°.

Main beam angle	Simulated side lobe level	Measured side lobe level
0°	−13 dB	−11 dB
5°	−12 dB	−10 dB
10°	−12 dB	−10 dB
15°	−15 dB	−9 dB
20°	−14 dB	−10 dB
25°	−11 dB	−10 dB
30°	−11 dB	−8 dB
35°	−11 dB	−10 dB
40°	−11 dB	−10 dB
45°	−13 dB	−12 dB
−5°	−12 dB	−10 dB
−10°	−12 dB	−10 dB
−15°	−15 dB	−9 dB
−20°	−14 dB	−9 dB
−25°	−11 dB	−9 dB
−30°	−11 dB	−9 dB
−35°	−11 dB	−10 dB
−40°	−11 dB	−10 dB
−45°	−13 dB	−8 dB

Table 1.
Comparison between simulated and measured main beam angle and side lobe level.

Antenna	Scanning range	No. of beam	Average step	No. of antenna
[10]	360°	6	60°	6
[11]	360°	12	30°	13
[12]	360°	4	90°	5
[13]	73°	4	18°	4
This work	**90°**	**19**	**5°**	**8**

Table 2.
Comparison with previously studied beamforming array antenna designs for indoor localization.

5. Conclusion

With the desire to improve the resolution of AoA-based indoor positioning system, this chapter has focused on the design of multi-port phased array antenna using the reflection type phase shifter. The studies demonstrate that the beamforming array antenna with two-way Wilkinson power divider that is able to limit the loss and increase the isolation between the output ports. In addition, the important part in the array, the reflection type phase shifter, can continuously control the phase shift in full 360° range with low insertion loss and small variation. The main beam of the array antenna can be steered in direction from −45 to 45°

with high resolution. This design can be commercially available for WLAN communication system in the frequency range from 2.424 to 2.484 GHz. This will facilitate an effective solution for indoor positioning system with high accurate localization. The future work will involve incorporating the phased array antenna for real positioning system for indoor object localization.

Acknowledgements

Conflict of interest

The author declares no conflict of interest.

Author details

Nguyen Thanh Huong[1,2]

1 School of Electrical Engineering, Hanoi University of Science and Technology, Hanoi, Vietnam

2 International Research Institute MICA, Hanoi University of Science and Technology, Hanoi, Vietnam

*Address all correspondence to: huong.nguyenthanh3@hust.edu.vn

IntechOpen

References

[1] Lee C, Chang Y, Park G, Ryu J, Jeong SG, Park S, Park JW, et al. Indoor positioning system based on incident angles of infrared emitters. In: Proceeding of 30th Annual Conference of IEEE Industrial Electronics Society, Vol. 3, 2004. IECON; 02 November 2004. pp. 2218-2222

[2] Feldmann S, Kyamakya K, Zapater A, Lue Z. An indoor bluetooth-based positioning system: Concept, implementation and experimental evaluation. In: International Conference on Wireless Networks. Vol. 272; 23 June 2003

[3] Li H. Low-cost 3D bluetooth indoor positioning with least square. Wireless Personal Communications. 2014;**78**(2): 1331-1344. DOI: 10.1007/s11277-014-1820-1

[4] Woo S, Jeong S, Mok E, Xia L, Choi C, Pyeon M, et al. Application of WiFi-based indoor positioning system for labor tracking at construction sites: A case study in Guangzhou MTR. Automation in Construction. 2011; **20**(1):3-13. DOI: 10.1016/j.autcon.2010.07.009

[5] Mazuelas S, Bahillo A, Lorenzo RM, Fernandez P, Lago FA, Garcia E, et al. Robust indoor positioning provided by real-time RSSI values in unmodified WLAN networks. IEEE Journal of Selected Topics in Signal Processing. 2009;**3**(5):821-831. DOI: 10.1109/JSTSP.2009.2029191

[6] Alarifi A, Al-Salman A, Alsaleh M, Alnafessah A, Al-Hadhrami S, Al-Ammar MA, et al. Ultra wideband indoor positioning technologies: Analysis and recent advances. Sensors. 2016;**16**(5): 707. DOI: 10.3390/s16050707

[7] Medina C, Segura JC, De la Torre A. Ultrasound indoor positioning system based on a low-power wireless sensor network providing sub-centimeter accuracy. Sensors. 2013;**13**(3): 3501-3526. DOI: 10.3390/s130303501

[8] De Angelis G, Pasku V, De Angelis A, Dionigi M, Mongiardo M, Moschitta A, et al. An indoor AC magnetic positioning system. IEEE Transactions on Instrumentation and Measurement. 2014;**64**(5):1267-1275. DOI: 10.1109/TIM.2014.2381353

[9] Rishabh I, Kimber D, Adcock J. Indoor localization using controlled ambient sounds. In: 2012 International Conference on Indoor Positioning and Indoor Navigation (IPIN); 13 November 2012. pp. 1-10

[10] Giorgetti G, Cidronali A, Gupta SK, Manes G. Single-anchor indoor localization using a switched-beam antenna. IEEE Communications Letters. 2009;**13**(1):58-60. DOI: 10.1109/LCOMM.2009.081584

[11] Rzymowski M, Woznica P, Kulas L. Single-anchor indoor localization using ESPAR antenna. IEEE Antennas and Wireless Propagation Letters. 2015;**15**: 1183-1186. DOI: 10.1109/LAWP.2015.2498950

[12] Kamarudin MR, Nechayev YI, Hall PS. Onbody diversity and angle-of-arrival measurement using a pattern switching antenna. IEEE Transactions on Antennas and Propagation. 2009; **57**(4):964-971. DOI: 10.1109/TAP.2009.2014597

[13] Bui TD, Le MT, Nguyen QC. Electronically steerable antenna array for indoor positioning system. Journal of Electromagnetic Waves and Applications. 2019;**33**(7):838-852. DOI: 10.1080/09205071.2018.1555060

[14] Mailloux RJ. Phased Array Antenna Handbook 3e. USA: Artech House; 2017. ISBN: 978-1-6308-102

[15] Balanis CA. Antenna Theory: Analysis and Design 4e. NY: John Wiley & Sons; 2016. ISBN: 978-1-118-64206-1

[16] Miroslav DL, Milan JL, Borislav OL. Analysis of SDMA & Smart Antenna Techniques for Existing and New Mobile Communication Systems. November 2003. Available from: http://www.telfor.org.yu/telfor2001/radovi/4-1.pdf

[17] Tseng CH, Chen CJ, Chu TH. A low-cost 60-GHz switched-beam patch antenna array with Butler matrix network. IEEE Antennas and Wireless Propagation Letters. 2008;**7**:432-435. DOI: 10.1109/LAWP.2008.2001849

[18] Chang CC, Lee RH, Shih TY. Design of a beam switching/steering Butler matrix for phased array system. IEEE Transactions on Antennas and Propagation. 2009;**58**(2):367-374. DOI: 10.1109/TAP.2009.2037693

[19] Denidni TA, Libar TE. Wide band four-port Butler matrix for switched multibeam antenna arrays. In: 14th IEEE Proceedings on Personal, Indoor and Mobile Radio Communications. Vol. 3. Beijing, China: PIMRC; 2003. pp. 2461-2464. DOI: 10.1109/PIMRC.2003.1259161

[20] Butler J. Beam-forming matrix simplifies design of electronically scanned antenna. Electronic Design. 1961;**9**:170-173

[21] Rabinovich V, Alexandrov N. Antenna Arrays and Automotive Applications. Germany: Springer Science & Business Media; 2012. DOI: 10.1007/978-1-4614-1074-4

[22] Pozar DM. Microwave Engineering 3e. NY: John Wiley & Sons; 2009. ISBN: 978-0-4706-3155-3

[23] Nguyen TH, Nguyen CT. Beamsteering phased array antenna using a full 360° and programmable continuous phase shifter for indoor localization. In: 2018 IEEE Seventh International Conference on Communications and Electronics (ICCE). 2018. pp. 227-230

[24] Lambard T, Lafond O, Himdi M, Jeuland H, Bolioli S. A novel analog 360° phase shifter design in Ku and Ka bands. Microwave and Optical Technology Letters. 2010;**52**(8):1733-1736. DOI: 10.1002/mop.25307

[25] Bulja S, Mirshekar-Syahkal D. Analysis and design of a new reflection-type 360° phase shifter with combined switch and varactor. Microwave and Optical Technology Letters. 2010;**52**(3): 530-535. DOI: 10.1002/mop.24975

[26] Burdin F, Iskandar Z, Podevin F, Ferrari P. Design of compact reflection-type phase shifters with high figure-of-merit. IEEE Transactions on Microwave Theory and Techniques. 2015;**63**(6): 1883-1893. DOI: 10.1109/TMTT.2015.2428242

[27] Wadell BC. Transmission Line Design Handbook. USA: Artech House; 1991.ISBN: 978-0-8900-6436-8

[28] Gardner DW, Wickert MA. Microwave filter design using radial line stubs. In: IEEE Region 5 Conference, 1988: 'Spanning the Peaks of Electrotechnology'. 1988. pp. 68-72

[29] Atwater HA. The design of the radial line stub: A useful microstrip circuit element. Microwave Journal. 1985;**28**:149-156

[30] Weijun L, Xiaojuan C, Xiaoxin L, Xiaolin M, Xinyu L, Xiaoliang W. A radial stub test circuit for microwave power devices. Chinese Journal of Semiconductors. 2006;**27**(9):1557-1561

[31] Sorrentino R, Roselli L. A new simple and accurate formula for microstrip radial stub. IEEE Microwave

and Guided Wave Letters. 1992;**2**(12): 480-482. DOI: 10.1109/75.173401

[32] Afridi MA. Microstrip patch antenna— designing at 2.4 GHz frequency. Biological and Chemical Research. 2015;**2015**:128-132

[33] Casu G, Moraru C, Kovacs A. Design and implementation of microstrip patch antenna array. In: 2014 10th International Conference on Communications (COMM). 2014. pp. 1-4

[34] Hong JS, Lancaster MJ. Microstrip Filters for RF/Microwave Applications. NY: John Wiley & Sons; 2004. DOI: 10.1002/9780470937297

[35] Bahl IJ. Lumped Elements for RF and Microwave Circuits. USA: Artech House; 2003. ISBN: 978-1-5805-3661-5

[36] SMV1247 SERIES Hyperabrupt Junction Tuning Varactor. Available from: https://www.skyworksinc.com/en/Products/Diodes/SMV1247-Series

[37] Zhang Z. Antenna Design for Mobile Devices. John Wiley & Sons; 2017. ISBN: 978-1-1191-3232-5